The Influence of the Quasi-Biennial Oscillation and El Niño-Southern Oscillation on the Northern Hemisphere Winter Stratospheric Polar Vortex

Peter Watson

First year report, August 2011

Supervised by Prof Lesley Gray

and Prof David Andrews

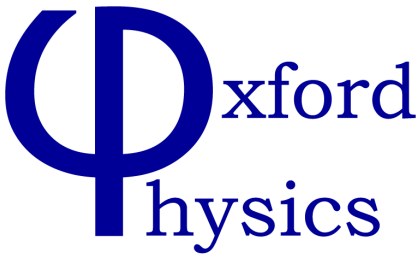

Atmospheric, Oceanic and Planetary Physics

Department of Physics

University of Oxford

Approx. 14,800 words

Abstract

This report presents details of my first year of reading a DPhil in Atmospheric, Oceanic and Planetary Physics. Current knowledge of the Northern Hemisphere winter stratospheric polar vortex and how it is influenced by the quasi-biennial oscillation (QBO) and the El Niño-Southern Oscillation (ENSO) is reviewed. Results from the Met Office HadGEM2-CCS general circulation model are presented. When the QBO and ENSO are assumed to influence the vortex separately, the model shows warming of the vortex during the easterly QBO phase (QBO-E) from late December through February and during warm ENSO events in March, in qualitative agreement with observations, although the model warming is weaker and later by around two months in each case. No strong evidence is found that the warming of the vortex by QBO-E is non-stationary in the model or in observations on decadal time scales. Further it is found that the QBO and ENSO combine to influence the vortex in a non-linear way in the model, such that the warming by QBO-E occurs earlier in the winter during the cold ENSO phase. Proposed future work to investigate this latter result is discussed.

Contents

1 Introduction

This year has been spent analysing variability of the Northern Hemisphere (NH) winter stratospheric polar vortex (hereafter "the vortex") in a stratosphere-resolving version of the Met Office Unified Model. The vortex exhibits a great deal of inter-annual variability which is not fully understood. Work in recent years has also suggested that vortex variability may influence weather at the surface, providing additional motivation for its study. The well-established influence of the quasi-biennial oscillation (QBO) in equatorial stratospheric winds on the vortex has been examined. The model that has been used includes an ocean that is coupled to the atmosphere, which is a recent development in models that resolve the stratosphere and allows the study of stratospheric variability under the influence of more realistic ocean variability. Therefore the influence of the El Niño-Southern Oscillation (ENSO), a major mode of ocean variability, on the vortex and the combined influence of the QBO and ENSO has also been studied.

Section 2 describes what is currently known about the vortex, the QBO, their interaction, which is called the Holton-Tan relationship (HTR) after Holton and Tan [1980] who were the first to record the connection, and the influence of ENSO on the vortex. Section 3 gives details of the observational data used, the Met Office Unified Model, the construction of an ENSO index for the model and the statistical methods used in the report. Section 4 shows results concerning the influence of the QBO and ENSO on the vortex in the Unified Model, section 5 gives some brief discussion and conclusions

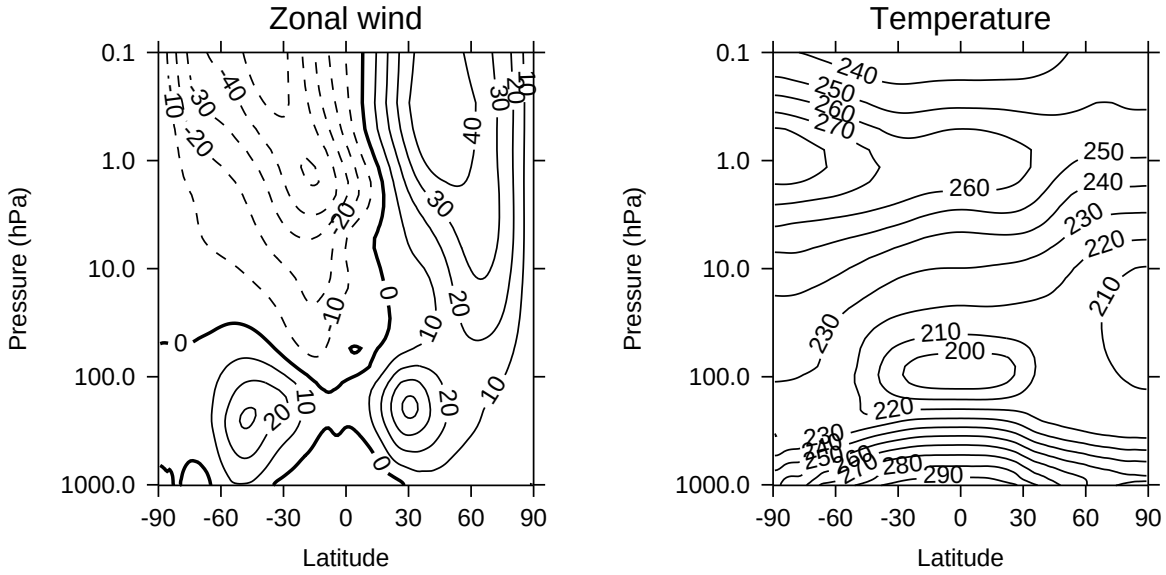

Figure 1: The DJF zonal mean zonal wind and temperature in ERA-40 and ECMWF Operational re-analysis for the period September 1957–August 2008.

of the report and section 6 explains my intended future work.

2 Background

2.1 The NH winter stratospheric polar vortex

Each NH winter the Arctic is plunged into the long polar night and the stratosphere cools by infrared radiation to space. This increases the Equator–Pole temperature gradient which increases the vertical wind shear in accordance with thermal wind balance and leads to a vortex of westerly winds forming in the stratosphere around the Arctic. The radiative-equilibrium state of the vortex therefore has a cold core of air above the Arctic circumscribed by a zonally-symmetric westerly jet [Shine, 1987]. Figure 1 shows the December-January-February (DJF) mean zonal mean zonal wind (ZMZW) and zonal mean temperature (ZMT) in the ERA-40 observational re-analysis (section 3.1). The westerly stratospheric vortex is visible in the NH, with the DJF ZMZW maximising between 0.1–1 hPa in mid-latitudes and maximising at 10 hPa near 60°N at $\sim$30 ms^{-1}, with a corresponding ZMT minimum of $\sim$210 K at the North Pole (NP) in the lower stratosphere. Whilst this is qualitatively similar to the radiative equilibrium state, the westerly vortex is less strong and and the NP lower stratosphere is warmer than would be the case in equilibrium, due to the action of planetary (Rossby) waves, described in more

detail below [Shine, 1987]. The ZMZW and ZMT are strongly coupled by the thermal wind equation so that a "strong" vortex has high ZMZW and low ZMT. Easterly winds are present in the Southern Hemisphere (SH) stratosphere and the troposphere exhibits mid-latitude westerly jets.

A recent analysis of the vortex climatology using the ERA-40 re-analysis is provided by Mitchell *et al.* [2011a]. They found that the ZMZW averaged over all winters peaks in late December at (60°N, 10 hPa) at $\sim$40 ms^{-1} and the mean 60–90°N cap ZMT at 10 hPa reaches a minimum of $\sim$200 K. The centroid of the vortex (the position of maximum potential vorticity (PV)) is normally found near (50°E, 80°N) and the vortex is elongated with an aspect ratio of $\sim$1.5. The vortex variability tends to be greater at higher altitudes due to increased wave activity, although it also becomes more circular as radiative timescales decrease and there is less distortion due to the Aleutian high (a region of climatologically high geopotential height in the stratosphere, centred near (175°W, 55°N) at 10 hPa and tilting westward with height [Harvey and Hitchman, 1996]). Westerly NH winds are present from about August until April.

Normally the radiative-equilibrium state is perturbed by planetary waves which introduce zonal asymmetry into the flow, and reduce the ZMZW and raise the ZMT. Figure 2 shows daily mean geopotential height (GPH) snapshots at 10 hPa. Figure 2(a) illustrates that typically low GPH, indicating cold air, is found over the pole and wave activity nudges the vortex shape away from circularity. The SH winter vortex is stronger and more stable than that in the NH, due to there being less planetary wave activity since there is less landmass [Baldwin *et al.*, 2003b].

Sometimes more major wave events result in large disturbances of the vortex called "stratospheric sudden warmings" (SSWs), resulting in a very zonally asymmetric flow [Andrews *et al.*, 1987]. Such an event is customarily defined as a reversal of the meridional ZMT gradient at 10 hPa or below between 60°N and 90°N. These are classified as "minor" if the ZMZW does not reverse and "major" if it does. Major SSWs are typically classified into two types: "vortex displacements" in which the vortex is displaced off the pole and distorted into a comma shape (figure 2(b)), and "vortex splits" during which the vortex separates into two separate cores of high PV air of comparable size (figure 2(c)). Charlton and Polvani [2007] found that major SSWs occur with a frequency of about 6 per decade in ERA-40, most frequently during January and February, with displacements and splits occurring with a frequency ratio of about 1.2:1. Several minor SSWs occur in the NH each year. However, the definition of an SSW and the classification into minor warmings, displacements and splits is somewhat arbitrary. Major SSWs can simultaneously show characteristics of displacements and splits, and some minor SSWs can appear more disruptive to the vortex than some major SSWs. Some recent work has focussed on

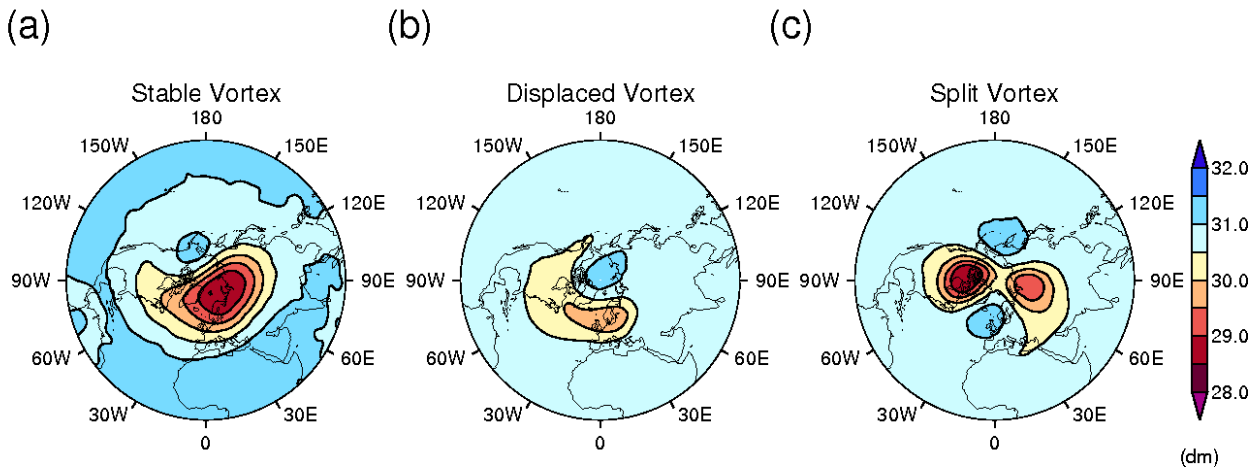

Figure 2: Daily averaged geopotential height fields for three different states of the NH polar vortex on the 10 hPa surface. (a) A stable vortex (01/12/81), (b) a displaced vortex (10/12/87), (c) a vortex that has split into two daughter vortices (29/12/84). Red shows cyclonic motion and blue shows anticyclonic motion. The units are geo-potential decameters and ERA-40 re-analysis data obtained from the British Atmospheric Data Centre were used. From Mitchell [2010], with permission.

explictly studying the vortex geometry during these events rather than zonal mean diagnostics in order to gain greater understanding [Waugh, 1997; Matthewman *et al.*, 2009; Mitchell *et al.*, 2011a; Hannachi *et al.*, 2011]. Coughlin and Gray [2009] showed that about 10% of days in the October–March period display a disturbed vortex, including all minor and major SSWs.

It is generally accepted that SSWs are associated with upward propagating planetary waves from the troposphere and their interaction with the mean flow [Andrews *et al.*, 1987]. Prior to the SSW occurring, there is a positive meridional heat flux in mid-latitudes at 100 hPa which is dominated by a zonal wavenumber-1 component in the case of displacements and by a zonal wavenumber-2 component in the case of splits [Charlton and Polvani, 2007]. The warming process is approximately adiabatic and associated with descending air at high latitudes, with air rising and cooling at low latitudes to compensate [Andrews *et al.*, 1987].

SSWs evolve over a period lasting around two–three months. Charlton and Polvani [2007] found evidence for "pre-conditioning" of the vortex prior to vortex splits, in which the vortex is confined further polewards than usual making it more susceptible to being disturbed by waves [McIntyre, 1982].

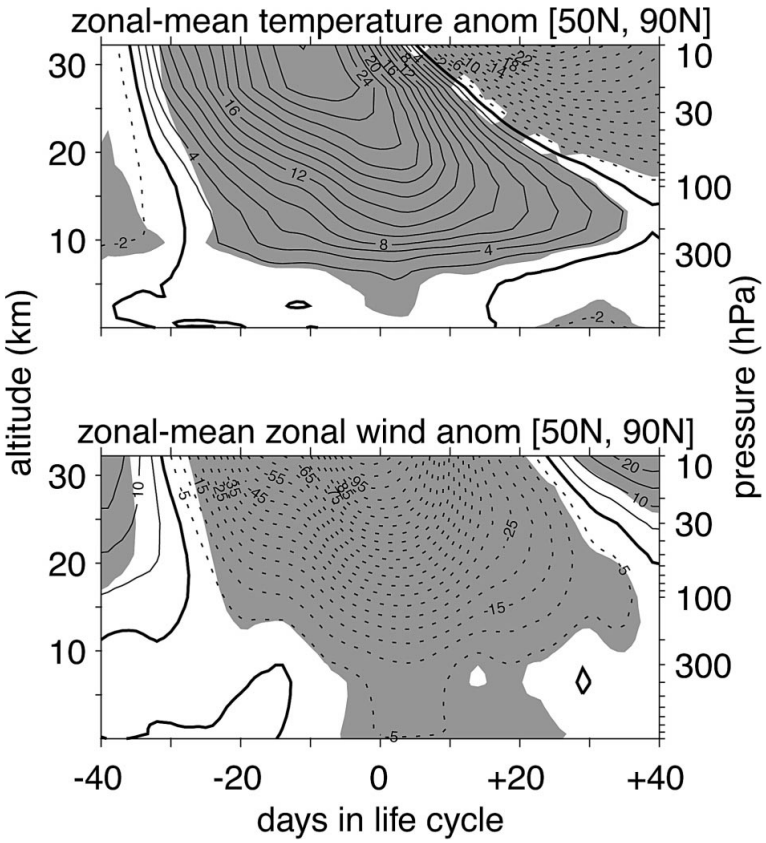

Figure 3: Zonal-mean temperature anomalies and zonal-mean zonal wind anomalies integrated poleward of 50°N during the composite life cycle of SSWs. Negative contours are given as dashes. Zero contours are given as a bold solid line. Contour interval for temperature (zonal wind) is 2 K (5 ms^{-1}). Dark gray shading indicates areas with a 95% confidence level (based on t statistics). From Limpasuvan *et al.* [2004].

Then during the warming, the 50–90°N 10 hPa polar cap ZMT rises by ∼10 K over ∼20 days and then falls again over roughly the next 30–40 days. Limpasuvan *et al.* [2004] show the ZMT and ZMZW anomalies propagate downwards with time, decaying as the ZMT anomaly maximum moves below 50 hPa and into the upper troposphere (figure 3). A cold anomaly is found above the warm anomaly, due to less wave activity reaching the upper stratosphere and mesosphere during a major SSW as the zonal wind becomes easterly, so that upwards stationary wave propagation is inhibited in accordance with the Charney-Drazin criterion [Charney and Drazin, 1961]. This descending cold anomaly means that at 10 hPa the ZMT averaged over the whole winter is not much affected by SSWs [Charlton and Polvani, 2007].

O'Sullivan and Salby [1990] showed the evolution of an SSW in a barotropic model. Beginning with a zonally-symmetric vortex, a tongue of high PV air is drawn out from the polar region and low PV mid-latitude air is drawn north, forming a region with a negative meridional PV gradient, which "rolls up" to form anticyclonic systems. These cause deviations from zonal symmetry in the vortex. Stronger planetary wave forcing leads to more intense stirring by these eddies, leading to a displacement-type event in their model. Gray *et al.* [2003] found in a primitive equation model of the stratosphere and mesosphere that anticyclones formed in the flow and merged with the Aleutian high, increasing its strength until a displacement event occurred.

In recent years evidence has accumulated indicating that vortex variability may affect the troposphere. Baldwin and Dunkerton [1999] and Baldwin and Dunkerton [2001] found evidence of downward propagation of the Northern Annular Mode signal from the troposphere to the stratosphere. Thompson *et al.* [2002] showed that weakenings of the vortex are associated with extreme cold events in eastern North America, northern Europe and eastern Asia. Ambaum and Hoskins [2002] argued that a stronger vortex raises the Arctic tropopause and that this may influence the North Atlantic oscillation (NAO), which is supported by the modelling study of Norton [2003]. Polvani and Kushner [2002] found that cooling the vortex in a primitive equation model led to the NH tropospheric jet shifting polewards and strengthening at the surface, although Chan and Plumb [2009] claimed this was a result of the time scales of tropospheric variability being too long – the strengthening was found by Baldwin [2003] in observational data, but not the poleward shift of the jet. Charlton *et al.* [2004] showed that changing stratospheric initial conditions in a numerical weather-prediction model affects the Arctic oscillation at the surface. Scaife *et al.* [2005] demonstrated that trends in stratospheric ZMZW can explain the observed increase in the NAO index since the 1960s. Scaife and Knight [2008] found that the SSW in January 2006 contributed to cold European temperatures at that time and Kolstad *et al.* [2010] and Thompson *et al.* [2010] found that the evolution of SSWs is connected with cold air outbreaks in the NH. Ineson and Scaife [2009], Bell *et al.* [2009] and Cagnazzo and Manzini [2009] argued that SSWs play a role in the response of European winter climate to ENSO. Thus understanding NH stratospheric variability may improve seasonal forecasts of NH weather [Baldwin *et al.*, 2003a; Charlton *et al.*, 2003; Shaw and Shepherd, 2008; Marshall and Scaife, 2009; Thompson *et al.*, 2010; Maycock *et al.*, 2011].

2.2 The QBO

The QBO is a phenomenon in the equatorial tropical stratosphere whereby the ZMZW direction on a given pressure level alternates between being easterly and westerly, with the easterly and westerly

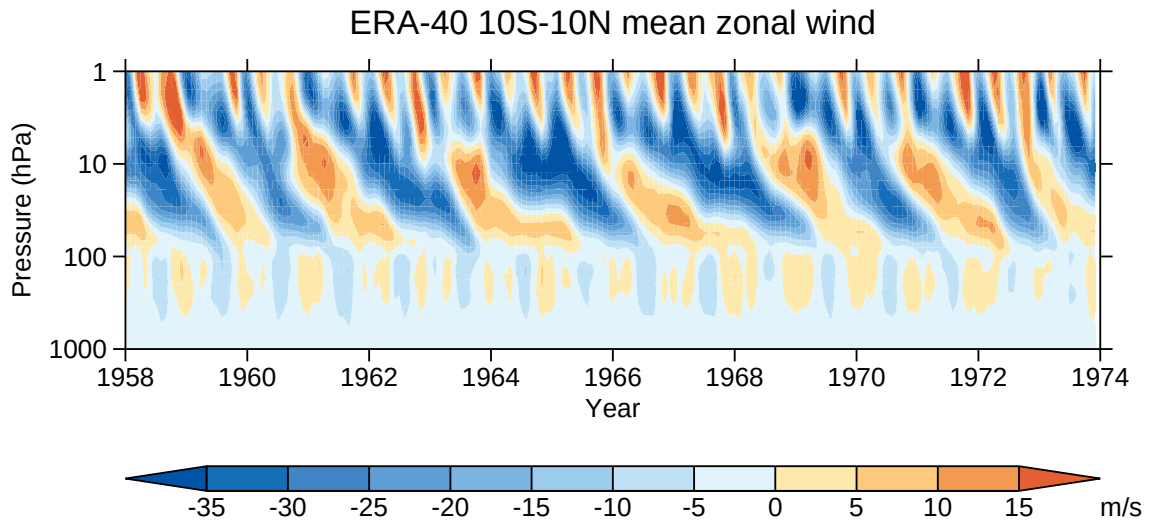

Figure 4: The 10S–10°N zonal mean zonal wind as a function of time and pressure in ERA-40, displaying the QBO. Produced by adapting code provided by S. Osprey.

wind regimes descending with time from the upper to the lower stratosphere. As each descends a new wind regime of opposite sign forms above and begins its descent. The average period is 28 months, which varies between 22–34 months for individual cycles [Baldwin *et al.*, 2001]. The QBO dominates variability of the equatorial stratosphere, as can be seen in figure 4 which shows a time series of the 10S–10°N mean ZMZW on all pressure levels in the ERA-40 re-analysis (see section 3.1) in which the QBO is clearly visible between 5–90 hPa. Pascoe *et al.* [2005] and Crooks and Gray [2005] found a QBO signal up to 1 hPa, although at this level variability is mostly due to the semi-annual oscillation. Below about 50 hPa, the QBO winds are close to being zonally symmetric, but at greater altitudes during the westerly phase, the propagation of planetary waves across the Equator can cause the zonal wind to vary with longitude [Hamilton, 1998]. The meridional half-width of the QBO is about 12°.

The easterly and westerly wind regimes are not symmetrical. The easterly winds are stronger than the westerlies, reaching about 20–25 ms^{-1} at 44 hPa compared to about 10–15 ms^{-1} for the westerly winds. The easterly wind regime descends more slowly, at a rate of about 2 hPa/month, than the westerly winds, which descend at about 4 hPa/month [Pascoe *et al.*, 2005].

This asymmetry in the descent rate is due to the presence of a meridional circulation associated with the QBO. The QBO is found empirically to be in thermal wind balance (despite occurring over the Equator) [Randel *et al.*, 1999], which implies the existence of a warm spot beneath the westerly

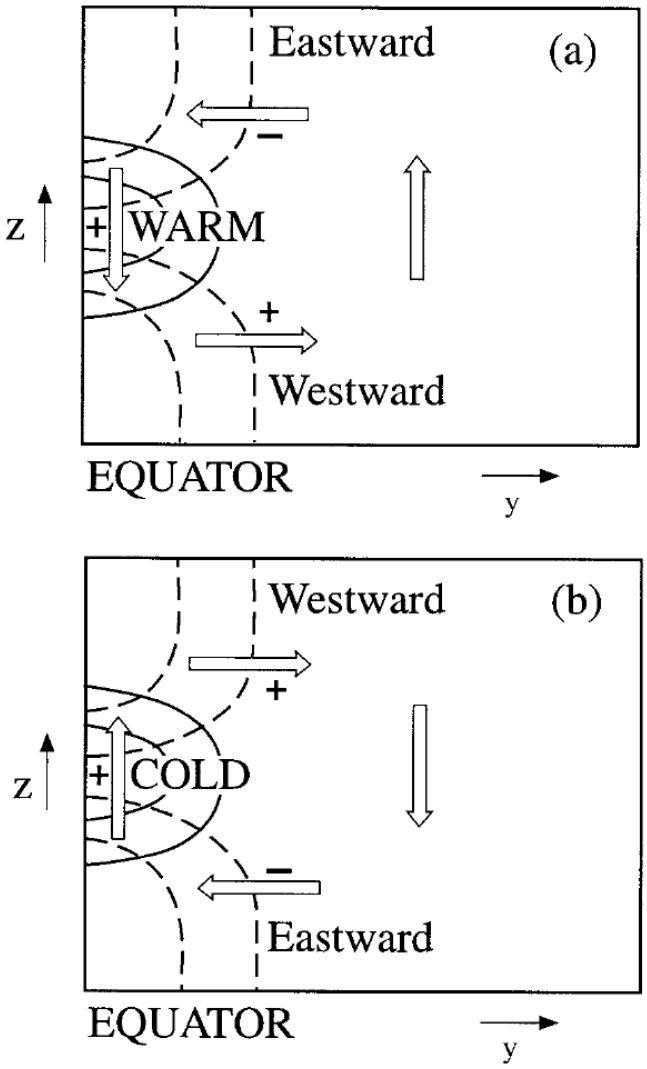

Figure 5: Schematic latitude-height sections showing the mean meridional circulation associated with the equatorial temperature anomaly of the QBO. Solid contours show temperature anomaly isotherms, and dashed contours are zonal wind isopleths. Plus and minus signs designate signs of zonal wind accelerations driven by the mean meridional circulation. (a) Westerly shear zone. (b) Easterly shear zone. After Plumb and Bell [1982].

winds and a cold spot beneath the easterlies. These are maintained by a combination of adiabatic heating/cooling by vertically-moving air and diabatic heating/cooling due to ozone variations brought about by this vertical motion [Plumb and Bell, 1982; Hasebe, 1994; Li *et al.*, 1995]. Thus the warm spot beneath the westerly winds is associated with descending air and the cold spot beneath the easterlies with ascending air, causing the westerly winds to descend more quickly. This is illustrated in figure 5.

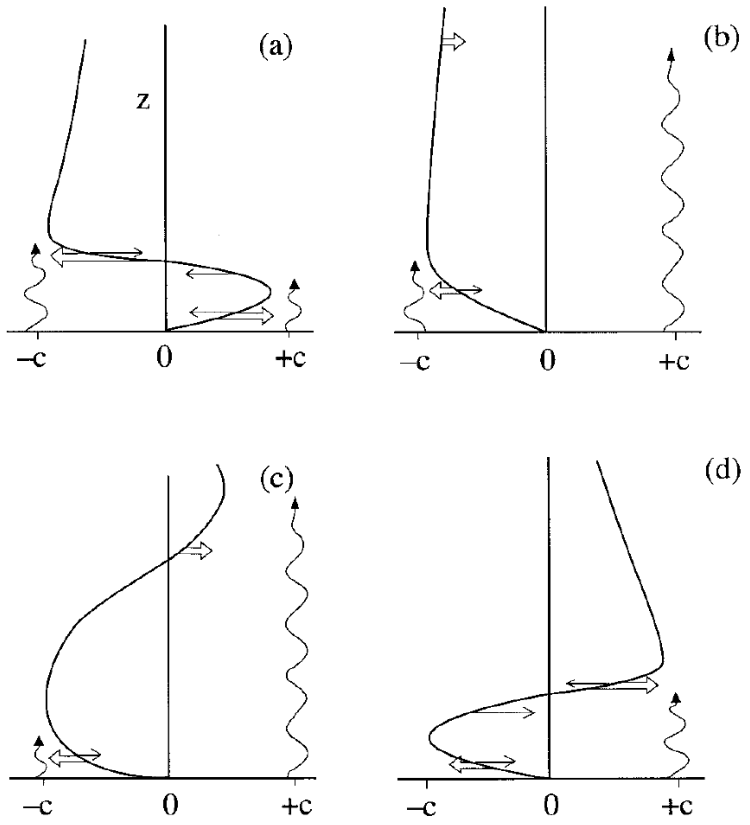

Figure 6: Schematic representation of the evolution of the mean flow in *Plumb's* [1984] analog of the QBO. Four stages of a half cycle are shown. Double arrows show wave-driven acceleration, and single arrows show viscously driven accelerations. Wavy lines indicate relative penetration of eastward and westward waves. After Plumb [1984].

The easterly wind descent is slowed so much that it stalls around 30 hPa in some years during northern winter, due to the equatorial upwelling associated with the Brewer-Dobson circulation sometimes being strong enough at that time to fully resist the downward descent of the winds (for example, in 1965 in figure 4) [Pascoe *et al.*, 2005]. This leads to seasonal locking of the westerly-to-easterly transition, which occurs more frequently during April–July at 44 hPa than in other months [Pascoe *et al.*, 2005]. The easterly-to-westerly transition exhibits seasonal locking to a lesser degree. The vertical motion at the Equator is part of a set of cells with vertical motion between about 20–40° of opposite sign to that at the Equator, and hence there are also temperature anomalies of opposite sign at these latitudes [Baldwin *et al.*, 2001].

Lindzen and Holton [1968] provided the first explanation of the QBO that is close to the modern understanding. Additional important contributions were made by Holton and Lindzen [1972], Plumb

[1977] and Plumb [1984]. Briefly, waves generated by deep convection and airflow over orography in the troposphere propagate upwards and are dissipated when they approach a "critical layer" where the zonal wind is close to the wave's zonal phase speed. Thus if easterly winds are present in the lower stratosphere, an easterly-propagating wave whose phase velocity is below that of the maximum easterly wind causes easterly acceleration just below the layer, schematically illustrated in figure 6. Meanwhile westerly-propagating waves pass through the easterly wind layer until they meet a layer of westerly winds greater than the waves' phase speed, causing westerly acceleration below this layer and above the layer of easterly winds. In this way the layer of easterly winds moves downwards, until it reaches the layer where wave forcing is generated. Here it is eroded by viscous dissipation as the westerly winds descend from above and increase the magnitude of $\partial^2 u/\partial z^2$. The process repeats with westerly winds in place of the easterlies until easterly winds are again present in the lower stratosphere, completing one QBO cycle.

According to this model, the period of the QBO is determined by the total upward momentum flux and the distance between the wave source and the region of the semi-annual oscillation, and the amplitude is limited by the maximum wave phase speed. Dunkerton [1997] argued that known fluxes of Kelvin, Rossby-gravity and gravity waves from the tropical troposphere are sufficient to explain the observed QBO period, and that laterally-propagating Rossby waves may also be important. The Coriolis effect, annual cycle and ozone advection are also important considerations for fully explaining the QBO [Dunkerton, 1997; Baldwin *et al.*, 2001].

Not all atmospheric models spontaneously produce a QBO. Important factors are having a fine vertical resolution in the stratosphere to better resolve short-wavelength gravity waves (although models with coarse vertical resolution may be able to produce a QBO, depending on the gravity wave parameterisation [L. Gray, pers. comm.]), a small diffusion coefficient to prevent smoothing of meridional gradients in the zonal wind and a sufficient upward wave momentum flux produced by convection [Baldwin *et al.*, 2001].

The state with easterly winds in the equatorial lower stratosphere and westerly winds above is termed QBO-E and that with westerly winds below and easterly winds above is termed QBO-W. The QBO phase may be defined in various ways, such as by using the sign of the wind on a particular pressure level or by applying Empirical Orthogonal Function (EOF) analysis (which is discussed in section 3.3).

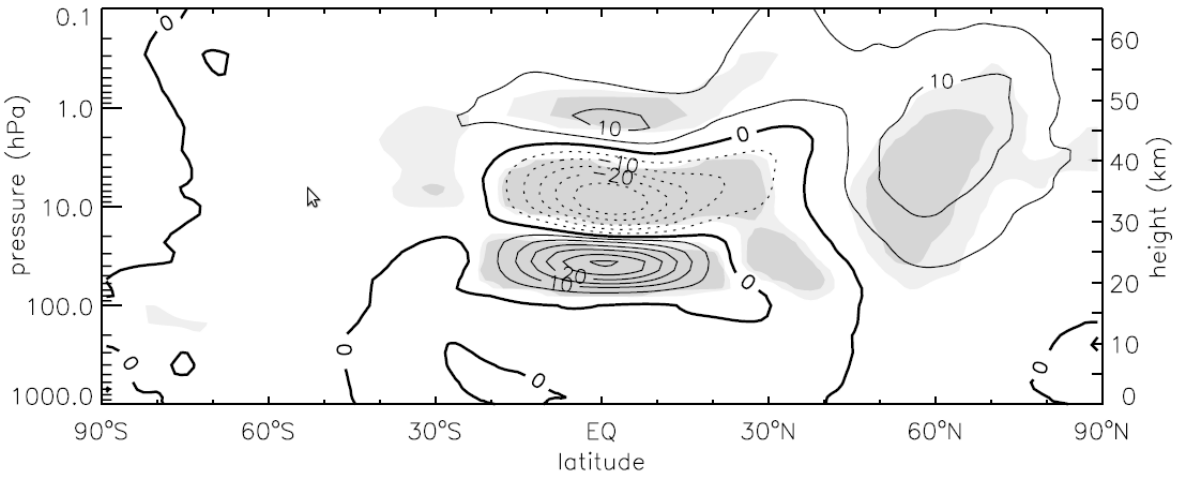

Figure 7: December–January zonal mean zonal wind difference for QBO-W minus QBO-E years with t test confidence shading shown at 95% and 99%; contours are at 5 ms^{-1} intervals. From Pascoe *et al.* [2005].

2.3 The Holton-Tan relationship

2.3.1 Observations and modelling studies

Numerous studies have found that the vortex is stronger when equatorial lower stratospheric winds are westerly than when they are easterly in observations dating from the late 1950s [Holton and Tan, 1980, 1982; Labitzke, 1982; Baldwin and Dunkerton, 1991; Dunkerton and Baldwin, 1991; Naito and Hirota, 1997; Baldwin and Dunkerton, 1998; Gray *et al.*, 2001b, 2004; Pascoe *et al.*, 2005; Ruzmaikin *et al.*, 2005; Camp and Tung, 2007b; Lu *et al.*, 2008; Yamashita *et al.*, 2011; Mitchell *et al.*, 2011b]. The relationship is strongest when equatorial winds near 40–50 hPa are used to define the QBO phase. The different observational studies generally agree on the magnitude of the QBO influence.

Lu *et al.* [2008] conducted one of the most recent analyses and studied a relatively long period 1958–2006 in the European Centre for Medium Range Weather Forecasting Re-Analysis (ERA-40) and operational analyses, and found that the mean Nov–Jan ZMZW at (60°N, 10 hPa) differs between QBO-W and QBO-E years by around 9 ms^{-1} and the ZMT of the polar lower stratosphere differs by up to about 4 K. The differences are largest in December and January, reaching ∼15 ms^{-1} and ∼5 K in (60°N, 10 hPa) ZMZW and lower stratospheric polar ZMT respectively. February also exhibits significant, but smaller, differences. The ZMZW and ZMT differences descend as winter advances and

in February a negative ZMT difference in the polar stratosphere above 10 hPa is present, similar to the pattern seen during SSWs (section 2.1). The correlation between November–March mean 50 hPa equatorial ZMZW and (54°N, 10 hPa) ZMZW between 1958–2006 is 0.64. Mitchell *et al.* [2011b] found that the vortex-integrated PV is less during QBO-E than during QBO-W from November through February and the vortex centroid is displaced more southwards in November.

In the latitude-height plane, the ZMZW difference in the northern extratropics between QBO-W and QBO-E is an unequal dipole, with small negative ZMZW differences south of ∼40–45°N [Dunkerton and Baldwin, 1991; Pascoe *et al.*, 2005] (figure 7). Dunkerton and Baldwin [1991] found that the "zero correlation" line moves northwards through the winter and Ruzmaikin *et al.* [2005] showed the GPH difference is very similar to the Northern Annular Mode, the first EOF of NH GPH [Thompson and Wallace, 1998, 2000].

The influence of the QBO on the SH vortex is less well studied. Baldwin and Dunkerton [1998] show the difference between QBO-W and QBO-E ZMZW is greatest in November near (70S, 5 hPa) where it reaches up to 14 ms^{-1}, with the QBO phases defined using EOF analysis, roughly corresponding to using the sign of equatorial ZMZW at 25 hPa. This is the period of breakdown of the SH vortex, when it is more sensitive to wave activity. The QBO influence in the SH is relatively short-lived compared to that in the NH.

The HTR has been replicated in a variety of models, including a barotropic model [O'Sullivan and Salby, 1990], primitive equation models of the stratosphere and mesosphere with imposed wavenumber-1 GPH forcing at the bottom boundary and with QBO winds represented by a simple analytical expression [Holton and Austin, 1991; O'Sullivan and Young, 1992; O'Sullivan and Dunkerton, 1994] and with equatorial winds relaxed to their observed values [Gray *et al.*, 2001a, 2003, 2004], in atmospheric general circulation models (GCMs) with an imposed QBO [Hamilton, 1998] and with a spontaneous QBO [Niwano and Takahashi, 1998; Calvo *et al.*, 2007; Marshall and Scaife, 2009; Anstey *et al.*, 2010] and in chemistry climate models with an imposed QBO [Yamashita *et al.*, 2011] and a spontaneous QBO [Naoe and Shibata, 2010], to give some examples. Therefore the presence of the HTR is robust and insensitive to the choice of model, the nature of the planetary wave forcing and the representation of the QBO. The HTR has not before been considered in a model with a dynamic ocean, which is used in this report (section 3.2), principally because including both a dynamic ocean and a well-resolved stratosphere in a GCM is very computationally expensive.

2.3.2 Mechanism

The most favoured theoretical explanation for the HTR is that the equatorial winds influence the waveguide for extratropical planetary waves. Stationary planetary waves are unable to propagate through easterly winds, and so when the QBO is in its easterly phase, waves are confined more strongly to NH middle and high latitudes and wave activity in these regions is stronger than when the QBO is in its westerly phase and waves only encounter easterly winds in the SH. Thus the vortex is more disturbed during QBO-E [Holton and Tan, 1980; Baldwin *et al.*, 2001]. O'Sullivan and Dunkerton [1994] argue that the observed influence on the vortex comes about due to the cumulative influence of waves over time. This mechanism correctly predicts that the HTR is strongest in winter months in the NH, when wave activity is strongest and can explain why the QBO influence on the SH vortex is only apparent during southern spring, as wave activity in the SH is weaker and less able to affect the strong SH vortex in mid-winter. It is also supported by observations of tropical ozone, which show evidence of stronger NH wave activity in winter during QBO-E [Hamilton, 1989].

Dunkerton and Baldwin [1991] found that the Eliassen-Palm (EP) flux, which is indicative of the direction and magnitude of planetary wave propagation [Andrews *et al.*, 1987], into the extratropical stratosphere is greater during QBO-E for November–January and less in March. The divergence of the EP flux was also found to be less during QBO-E, suggesting the acceleration of the westerly vortex winds is less strong. However, no large differences between the frequency and characteristics of individual wave events during the two QBO phases were found. Ruzmaikin *et al.* [2005] found the wavenumber-1 component of the vertical component of EP flux is greater during QBO-E in November and early December and greater during QBO-W in late January and early February. The wavenumber-2 component is greater during QBO-E in late February and March. These results are on the whole consistent with the above theoretical explanation.

However, Naoe and Shibata [2010] and Yamashita *et al.* [2011] found in observations and a chemistry climate model that the mid-latitude lower stratospheric EP flux is directed more equatorward during QBO-E than during QBO-W and only more poleward at low latitudes, which contradicts this explanation. This result can also be seen in the analysis of Dunkerton and Baldwin [1991].

Yamashita *et al.* [2011] propose a modification of the waveguide explanation to account for this. Briefly, they suggest that during QBO-W, the lower stratospheric EP flux is more equatorward and this creates an EP flux divergence anomaly near 30°N, and the opposite occurs in the upper stratosphere due to the presence of the nascent QBO-E phase. These EP fluxes are associated with a meridional circulation which leads to adiabatic heating at 30°N, which strengthens the vortex during QBO-W

by increasing the Equator–Pole temperature gradient through the thermal wind relationship. This provides a role for upper stratospheric winds in the HTR mechanism. However, it should be borne in mind that these analyses only consider seasonally-averaged EP fluxes and are only diagnostic, so that causality cannot be established. Small EP flux anomalies also do not have a straightforward interpretation in terms of wave propagation [D. Andrews, pers. comm.].

There is also evidence from observational and modelling studies that upper stratospheric winds and wind shear play a role in the HTR mechanism. This could be important for explaining the observed modulation of the HTR strength by the 11-year solar cycle [Labitzke, 2005; Camp and Tung, 2007b]. Gray *et al.* [2001b] found the anticorrelation of winter polar stratospheric ZMT with equatorial upper stratospheric vertical wind shear in autumn is greater than that with equatorial lower stratospheric winds at any time, although they only had a limited amount of rocketsonde data available. Gray *et al.* [2001a] found in a stratosphere-mesosphere model that it was necessary to include equatorial upper stratospheric winds along with the lower stratospheric winds to reproduce the HTR. Gray [2003] demonstrated in the same model that equatorial lower stratospheric winds influenced the vortex in early winter and upper stratospheric winds had an influence in late winter. Matthes *et al.* [2004] found that equatorial upper stratospheric winds needed to be taken into account to reproduce the effect of the solar cycle on the vortex in an atmospheric GCM. These studies were highly simplified compared to the real atmosphere, however.

Ruzmaikin *et al.* [2005] found in re-analysis data that the meridional circulation associated with the QBO can extend to NH high latitudes during winter, similar to the modelling result of Kinnersley and Tung [1999], and suggest that it may directly influence the high-latitude winds. Naoe and Shibata [2010] also argue the meridional circulation plays a role on the basis of their EP flux analysis, although, as described above, Yamashita *et al.* [2011] argue that this can still be explained in terms of modulation of planetary wave fluxes by the equatorial zonal wind. Garfinkel *et al.* [2011] conclude from a set of idealised GCM experiments that it is the meridional circulation and not the location of easterly winds which influences planetary wave propagation.

Overall, therefore, the consensus is that the equatorial winds influence the vortex by modulating NH planetary wave flux, although open questions remain about the role of equatorial upper stratospheric winds and the QBO meridional circulation.

The response of the vortex to planetary wave forcing is likely to be non-linear, which may be important for understanding the results presented in this report. Holton and Austin [1991] and O'Sullivan and Young [1992] found that sensitivity of the vortex in their models to the equatorial winds is small

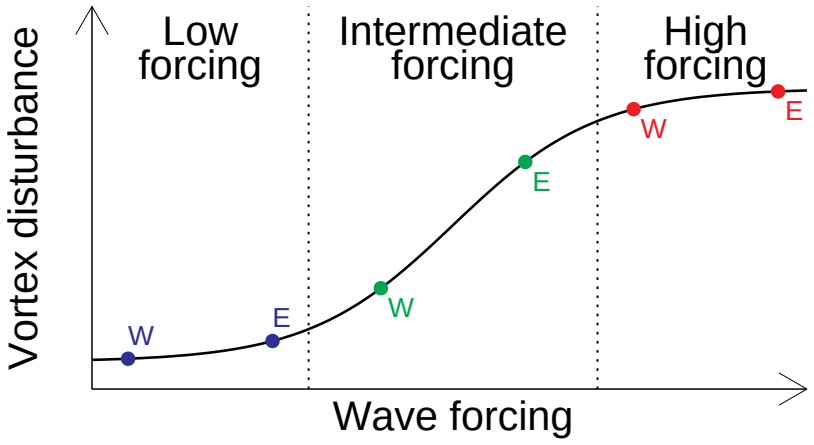

Figure 8: A simple illustration of how the climatological vortex state may influence the strength of the Holton-Tan relationship. The response of the vortex to changing wave forcing varies so that when the forcing is low (high), the vortex is undisturbed (disturbed) and is insensitive to changes in the level of the forcing, but there exists a range of intermediate forcing for which the vortex is much more sensitive. Thus in the low or high forcing regimes (blue and red dots respectively), the increase in the effective wave forcing between the QBO-E and QBO-W phases does little to change the mean vortex state compared to the effect in the intermediate regime (green dots). For simplicity the effective wave forcing difference between QBO-E and QBO-W is taken to be constant, although in reality it could also vary with the climatology. Note that this conceptual model supposes that the "vortex disturbance" over the winter can be represented by a scalar quantity, for example the seasonal mean polar cap temperature, in which case it has nothing to say about the timing of wave events.

when wave forcing is very small or very large and greatest when the forcing is intermediate. O'Sullivan and Dunkerton [1994] found evidence of a bifurcation in the vortex state, whereby below a threshold forcing, SSWs did not occur and above the threshold the vortex was considerably more disturbed. Inclusion of a seasonal cycle smoothed this bifurcation, and Gray *et al.* [2003] found a smoother transition between the low-forcing low-variability and large-forcing large-variability vortex regimes, where making the equatorial winds more easterly had an equivalent effect on the vortex to raising the wave forcing. This explains the results of Holton and Austin [1991] and O'Sullivan and Young [1992] as at low levels of direct forcing, the influence of the QBO-E phase is not great enough to cause disturbances in the vortex, and at large levels of forcing, the vortex is very variable even during QBO-W, so that

in each case the QBO has little influence. It is only when the direct forcing is near the bifurcation point that sensitivity of the vortex to the QBO influence is large. This is illustrated schematically in figure 8. However, it should be borne in mind that these studies used stratospheric models with highly simplified and controlled planetary wave forcings and representations of equatorial wind, and more complex models and the real atmosphere may display different behaviour.

This non-linear behaviour means that observations and different models cannot always be easily compared because, for example, a model may simulate the equatorial wind influence on propagating planetary waves correctly but predict an incorrect strength of the HTR due to a climatological bias in wave forcing or the vortex. Various differences between models or between models and the real atmosphere may combine to produce differences between the modelled and observed HTRs, or cancel out to give good agreement despite differences in the underlying processes.

2.4 Influence of ENSO on the vortex

ENSO is one of the largest modes of variability in the climate system. It is an irregular oscillation of tropical Pacific sea surface temperatures (SSTs) and sea level pressure with a period of 2–7 years. Climatologically the Pacific is colder in the east than in the west and the air pressure is higher in the east. During an El Niño (or warm ENSO, hereafter "WENSO") event, the eastern Pacific warms and air mass shifts from east to west, and the opposite occurs during La Niña (or cold ENSO, hereafter "CENSO") events [Cane, 2005; Brönnimann, 2007].

It is only fairly recently that the influence of ENSO on the vortex has been established, with most observational studies now agreeing that the mean vortex temperature over the winter is greater during WENSO than during CENSO by about the same as the difference between QBO-E and QBO-W winters [Wallace and Chang, 1982; van Loon and Labitzke, 1987; Labitzke and Van Loon, 1989; Baldwin and O'Sullivan, 1995; Kodera *et al.*, 1996; Chen *et al.*, 2003; Brönnimann *et al.*, 2004; Fernández *et al.*, 2004; Brönnimann, 2007; Camp and Tung, 2007a; Garfinkel and Hartmann, 2007; Wei *et al.*, 2007; Free and Seidel, 2009; Butler and Polvani, 2011; Mitchell *et al.*, 2011b; Ren *et al.*, 2011], although the results of the earliest studies were not robust due to the short length of the observational record and the difficulty of separating out the effects of other forcings [Hamilton, 1993a]. Mitchell *et al.* [2011b] found that the vortex has a lower integrated potential vorticity relative to climatology from December through March above approximately the 10 hPa level and in February and March below. The vortex ZMZW is also lower and it is displaced further south during WENSO in January and February. CENSO gives rise to opposite but smaller anomalies. ENSO's influence on the vortex is apparent later in the winter than

that of the QBO. Butler and Polvani [2011] found that SSWs are more frequent during both large WENSO and CENSO events than in neutral ENSO years, although the statistical significance of this result is not high. Garfinkel and Hartmann [2008] found that a weakened vortex is associated with an enhanced Pacific-North American pattern, which increases wavenumber-1 planetary wave flux into the stratosphere and occurs more frequently during WENSO events, and not with other tropospheric ENSO teleconnections.

Most modelling studies have found that WENSO events warm the vortex through the enhancement of wavenumber-1 planetary wave forcing into the stratosphere [Hamilton, 1993b; Sassi *et al.*, 2004; Garcia-Herrera *et al.*, 2006; Manzini *et al.*, 2006; Taguchi and Hartmann, 2006; Brönnimann *et al.*, 2006; Calvo *et al.*, 2008; Fischer *et al.*, 2008; Ineson and Scaife, 2009; Bell *et al.*, 2009; Cagnazzo and Manzini, 2009; Calvo *et al.*, 2009; Fletcher and Kushner, 2011; Lu *et al.*, 2011], although Lahoz [2000] did not find a clear signal. Sassi *et al.* [2004], Garcia-Herrera *et al.* [2006] and Manzini *et al.* [2006] also found that CENSO produced smaller anomalies relative to climatology than WENSO. Smith *et al.* [2010] found that increased Eurasian snow cover disturbs the vortex by the same mechanism, and that generally a tropospheric source of GPH anomalies will warm the vortex if a superposition of the anomalies and the climatological wave forcing gives positive interference, which is the case during WENSO events [Manzini *et al.*, 2006; Garfinkel and Hartmann, 2008; Garfinkel *et al.*, 2010].

There is observational and modelling evidence that the QBO and ENSO influences on the vortex interact non-linearly. Garfinkel and Hartmann [2007] found in observations that the influence of ENSO is diminished during QBO-E (as did Free and Seidel [2009]) and that of the QBO is diminished during WENSO, and Wei *et al.* [2007] found that the HTR is only significant during CENSO. Garfinkel and Hartmann [2010] suggested the QBO may alter the tropospheric ENSO teleconnection patterns and hence its influence on the vortex, although a portion of the observed effect could be due to sampling variability. Calvo *et al.* [2009] found in an atmospheric GCM that during the QBO-E phase, the warming of the vortex by WENSO is larger during December and January than during QBO-W, and that during WENSO periods, the warming of the vortex by QBO-E is greater and propagates downwards more quickly than during CENSO periods. Richter *et al.* [2011] found in a chemistry climate model that the SSW frequency is similar when either or both of QBO and ENSO variability are represented, but decreases considerably when neither is present. In addition, Hurwitz *et al.* [2011] found in observations that "warm pool" WENSO events warm the SH vortex in November–December only during QBO-E, suggesting this non-linearity is present in both hemispheres.

These results are consistent with the non-linearity of the vortex response to planetary wave forcing

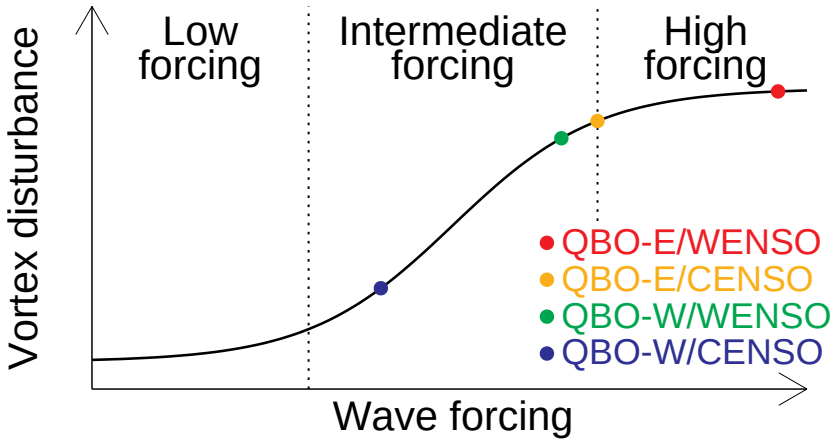

Figure 9: An illustration of how the QBO and ENSO may combine to influence the vortex, and how the difference in vortex state between QBO-E and QBO-W depends on the ENSO phase and how that between WENSO and CENSO depends on the QBO phase, guided by observational results (see text). The sensitivity of the vortex state to changes in wave forcing varies as in figure 8. The mean vortex state in QBO-W/CENSO winters is the "least disturbed", below the forcing level at which the vortex is very sensitive to wave forcing. Imposing either a QBO-E or WENSO forcing perturbation disturbs the vortex considerably. However, the sensitivity of the vortex state to changes in wave forcing is now less so that imposing the two perturbations in combination does less to raise the vortex disturbance further. Thus the QBO-E/CENSO minus QBO-W/CENSO disturbance difference is greater than the QBO-E/WENSO minus QBO-W/WENSO difference and the QBO-W/WENSO minus QBO-W/CENSO difference is greater than the QBO-E/WENSO minus QBO-E/CENSO difference.

in relatively simple models (section 2.3.2 and figure 8). WENSO causes greater wave forcing, so the vortex could move from the intermediate to the high forcing regime so that the QBO has less influence, or be moved from the low into the intermediate forcing regime so that the QBO has greater influence, depending on the climatology and the wave forcing produced under WENSO. Similarly during QBO-E the wave forcing is effectively increased, which may mean that the vortex is moved from the intermediate to the high forcing regime so that the ENSO phase has little influence, or from the low to the intermediate forcing regime so that ENSO's influence is increased, again depending on the climatology. If this idea is correct then the observational results suggest that the vortex is close to the high-forcing regime during either QBO-E or WENSO (figure 9). This seems consistent with the results

of Richter *et al.* [2011], but the model of Calvo *et al.* [2009] would need to be in a low forcing regime in winters with neither QBO-E nor WENSO in order to be consistent.

A clear prediction of this explanation is that winters with combined QBO-W and CENSO phases should exhibit a "least-disturbed state" of the vortex, such as has been found in the case of winters with combined QBO-W and solar cycle minimum [Camp and Tung, 2007b], so that any perturbation by more easterly equatorial winds or WENSO conditions either makes the vortex more disturbed or has little effect.

3 Data and methods

3.1 The ERA-40 re-analysis

To evaluate the performance of the Met Office model used here at representing the real atmosphere, its output is compared to re-analysis produced by the European Centre for Medium-Range Weather Forecasts (ECMWF), including the ECMWF Re-Analysis (ERA-40) and ECMWF operational analysis up to September 2008. ERA-40 is a re-analysis produced using 3D-Var data assimilation to output the most likely state of the atmosphere at each 6 hour interval from September 1957 to August 2002 up to 0.1 hPa [Uppala *et al.*, 2005]. The process of 3D-Var data assimilation involves initialising a model at the start of the re-analysis period from observations, stepping the model forward in time and then combining the model output with observations to re-initialise the model at the beginning of the next timestep with a state that minimises a cost function of the discrepancy between this state and the observations and last model state, where the latter are weighted according to estimates of their errors. The input observations include surface measurements, radiosondes, flight data and satellite data from the 1970s onwards. As the number of available observations increased over the period of the re-analysis, the quality improved over time.

The ERA-40 representation of the QBO and SAO has been found to agree closely with independent rawinsonde and rocketsonde data up to 2–3 hPa [Baldwin and Gray, 2005]. Charlton and Polvani [2007] found the occurrence of SSWs in ERA-40 generally agreed with independent studies of individual SSWs and with the National Centers for Environmental Prediction–National Center for Atmospheric Research (NCEP–NCAR) re-analysis. Thus we can be confident that ERA-40 gives a good representation of stratospheric variability. ERA-40 has a known upper stratospheric temperature bias, being overly warm by several Kelvin early in the period and overly cold later [Uppala *et al.*, 2005]. Removing a linear trend from the data will lessen the effect of time-varying biases such as this. In the final years

there is an "unrealistic oscillatory temperature structure in the vertical in polar regions" during winter and spring [Uppala *et al.*, 2005].

3.2 The Met Office high top model

This report presents analysis of data produced by the Met Office HadGEM2-CCS GCM. This is a coupled ocean-troposphere-stratosphere model with 60 atmospheric levels in the vertical up to 84km altitude (corresponding to a pressure of approximately 0.01 hPa), with 32 levels above 16km (corresponding approximately to a pressure of 100 hPa), with atmospheric horizontal resolution 1.25° in latitude and 1.875° in longitude. The model includes parameterised non-orographic gravity wave drag, which causes the model to exhibit a spontaneous QBO. The model does not include a chemistry scheme, apart from parameterised methane oxidation, although it includes a coupled carbon cycle. These and other model details can be found in Martin *et al.* [2011].

The results presented in this report are from a 240-year control run of HadGEM2-CCS. The control run does not include time-varying forcings such as anthropogenic greenhouse gas and aerosol emissions, volcanic eruptions or the eleven-year solar cycle and the vortex would only be expected to be affected by the QBO (section 2.3), ENSO (section 2.4) and Eurasian snow cover [Cohen *et al.*, 2007; Allen and Zender, 2010; Smith *et al.*, 2010; Schimanke *et al.*, 2010]. This means the impact of the QBO and ENSO on the vortex is more easily distinguished and a greater statistical significance can be attained than if the historical runs that include the other forcings were used. A zonal mean seasonal cycle of pre-industrial ozone concentrations is prescribed [S. Osprey, pers. comm.].

Osprey *et al.* [2011] found that HadGEM2-CCS exhibits a realistic stratospheric climatology and realistic variability. The DJF mean ZMZW is similar to that in ERA-40. The model has a warm bias in the tropical lower stratosphere, a cold bias in the tropical upper stratosphere of 2–6 K and a warm bias of up to 4 K in the DJF high latitude NH stratosphere. The (60°N, 10 hPa) ZMZW shows a realistic seasonal cycle and variability through the northern winter [Hardiman *et al.*, 2011]. The modelled vortex covers a smaller area than in ERA-40, but has a realistic aspect ratio and centroid latitude [D. Mitchell, pers. comm.].

The overall SSW frequency is consistent with that in ERA-40, although SSWs occur less frequently in November–January and more frequently in February–March [Osprey *et al.*, 2011]. This is consistent with the planetary wave forcing being slightly weaker than that in ERA-40 – Osprey *et al.* [2010] found the peak standard deviation in GPH at 10 hPa in an atmosphere-only version of this model's predecessor, HadGEM, to be weaker by 10% and the wave activity to be weaker in late winter, which

is unlikely to be very different in HadGEM2-CCS [S. Osprey, pers. comm.]. The distribution in time and height of model final warming dates is similar to that in observations. The model produces a realistic "tropical tape recorder" of equatorial stratospheric water vapour concentrations and realistic stratospheric "age of air", indicating that the model Brewer-Dobson circulation and stratospheric extratropical variability are realistic [Osprey *et al.*, 2011].

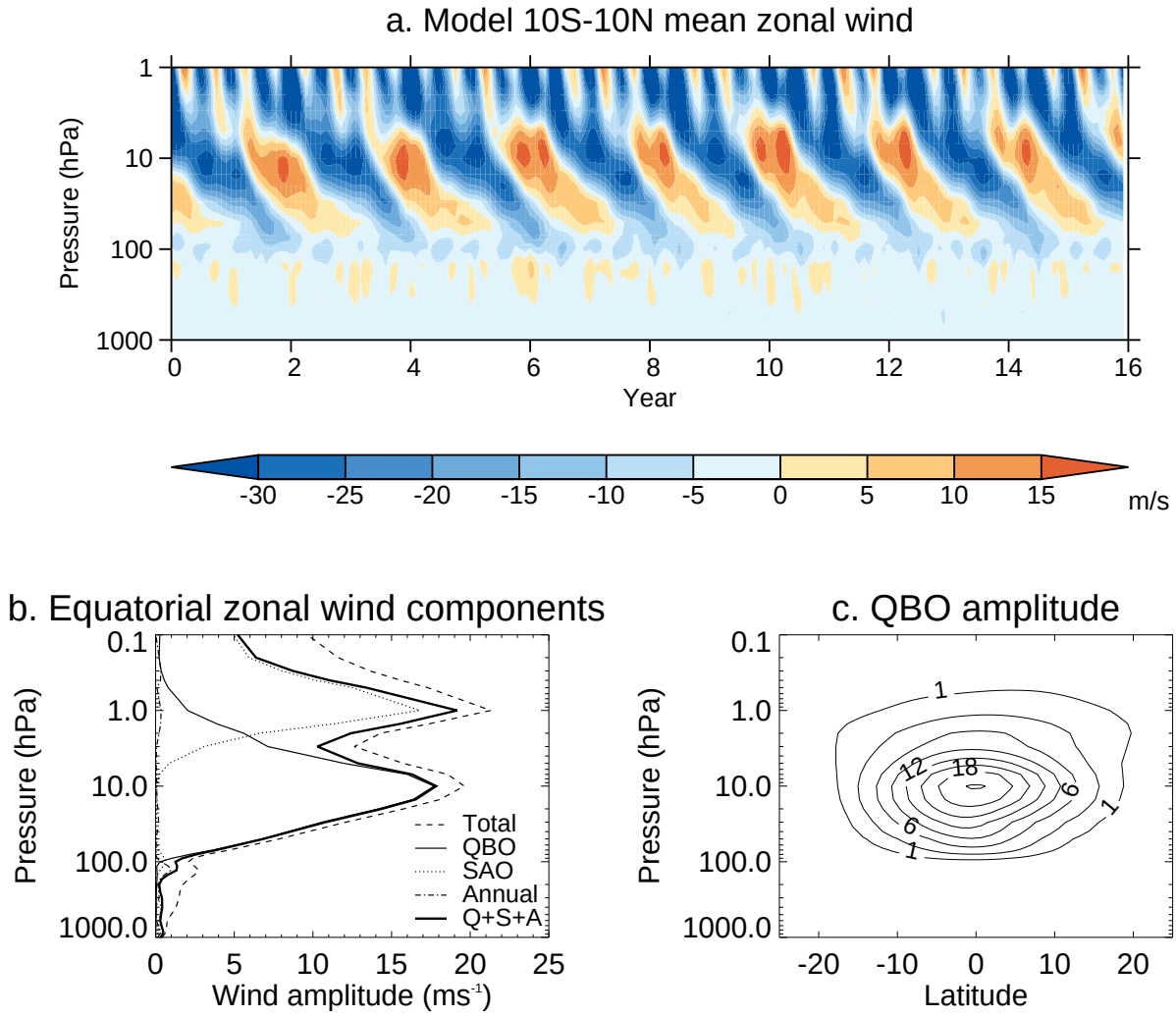

Figure 10: The QBO in the Met Office model. (a) shows the monthly, 10S–10°N and zonal mean zonal wind as a function of time and pressure. (b) shows the amplitude of the QBO, SAO and annual cycle components of the 10S–10°N zonal mean zonal wind (see text). (c) shows the amplitude of the QBO as a function of latitude and pressure in ms^{-1}. Produced by adapting code provided by S. Osprey.

3.2.1 The QBO in the model

Figure 10(a) shows the 10S–10°N ZMZW as a function of height and pressure in the model. The modelled QBO closely resembles that in observations, with comparable maximum easterly and westerly ZMZW. The mean QBO period (defined by the time between successive westerly to easterly transitions at 50 hPa with a five month running mean applied to the ZMZW time series) in the model is 26.4 months, which is close to the observed period of 28.0 months. The modelled QBO is more regular than that in observations, as can be seen by comparing figures 4 and 10(a) and also from the fact that the standard deviation of the model QBO period is 1.8 months, compared to 3.9 months in ERA-40.

Figures 10(b) and (c) show some properties of the QBO in the model data, which can be compared to the similar analysis of Pascoe *et al.* [2005] of the QBO in ERA-40. They defined the QBO component of equatorial[1] winds to be the sum of the Fourier harmonics of the ZMZW with periods between 22–40 months, which dominate in the equatorial lower stratosphere. For the model data, I included all harmonics of 10S–10°N ZMZW in the spectral band centred near the mean period with amplitudes greater than 1m around the 10 hPa level, which corresponds approximately to the amplitude cut-off used by Pascoe *et al.* [2005], which included periods in the range 22–34 months. Other important components of the equatorial winds are the SAO and annual cycle, which correspond to the Fourier components with frequencies of exactly six and twelve months respectively.

Figure 10(b) shows the amplitude of all three components as a function of pressure. The model QBO amplitude peaks at approximately 18 ms^{-1} at 10 hPa, which is slightly higher than the peak amplitude in ERA-40, which is approximately 16 ms^{-1} at 15 hPa. The model QBO has a slightly greater amplitude at the uppermost levels than ERA-40 and a similar amplitude in the lower stratosphere, penetrating down to about 100 hPa. The model SAO also has a larger peak than in ERA-40, at about 17 ms^{-1} compared to 11 ms^{-1} in ERA-40 at 1 hPa, although it falls away with height more quickly so that both the model and ERA-40 SAO amplitudes are zero at 10 hPa and 5 ms^{-1} at 0.1 hPa. ERA-40 shows an annual cycle signal on levels 1–5 hPa peaking at about 4 ms^{-1} and on levels 100–500 hPa peaking at about 3 ms^{-1} which is not captured by the model.

Figure 10(c) shows the amplitude of the model QBO as a function of latitude and height. The amplitude peaks at 21 ms^{-1} at 10 hPa at the Equator and decreases with latitude to be about 1 ms^{-1} at 20°S and 20°N, being fairly symmetric about the Equator. The corresponding figure for ERA-40 [Pascoe *et al.*, 2005, fig. 4a] appears similar, but with a smaller peak amplitude of about 15 ms^{-1} and a smaller amplitude at higher levels.

[1] Pascoe *et al.* [2005] neglect to state what latitude range "equatorial" corresponds to.

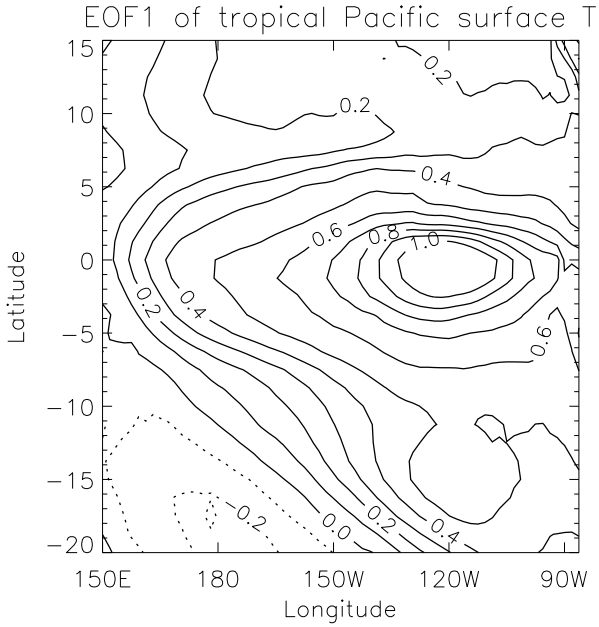

Figure 11: The first EOF of tropical Pacific surface temperature, showing the temperature change in K associated with a one standard deviation increase in the corresponding principal component.

Overall, therefore, the model QBO has a realistic meridional structure and mean period, with a slightly greater amplitude in the middle and upper stratosphere and a more regular descent than in ERA-40.

3.3 Constructing an ENSO index

HadGEM2 has been found to simulate a realistic ENSO, albeit with peak variability at slightly longer time scales than in observations [Collins *et al.*, 2008]. For observational data, the SST anomaly in a particular region of the tropical Pacific is commonly used as an ENSO index. However, GCMs generally exhibit biases in the spatial structure of tropical Pacific SST variability that may make the regions used for observations unsuitable for analysing ENSO in a model [Leloup *et al.*, 2008]. Therefore in this work I have used the principal component (PC) of the first Empirical Orthogonal Function (EOF) of Pacific surface temperature variability in the region (150°E–85°W, 20°S–15°N), where the variability is large.

To construct the first EOF of a dataset, each spatial element of the data is considered to be one element of the data vector that represents the spatial structure of the data at a given time. The first EOF is the leading eigenvector of the covariance matrix of this data vector. The first PC is the

scalar product of the data vector with the first EOF at each time step. The first EOF can often be associated with a known physical process [von Storch and Zwiers, 1999]. In this work I have made use of M. Baldwin's IDL script eofcalc to compute EOFs (http://www.nwra.com/resumes/baldwin/eofcalc.pro).

The first EOF is constructed using deseasonalised monthly-mean surface temperature data and captures 43% of the variance in surface temperature in the region (150°E–85°W, 20°S–15°N) (figure 11). It exhibits a "tongue" structure across the tropical Pacific, with a maximum near 120W, which is characteristic of ENSO variability [Brönnimann, 2007]. The first PC and EOF were found to be insensitive to varying the borders of this region. The PC was smoothed with a 5 month centred moving average to remove short-term variability unassociated with ENSO.

In order to check that the results in section 4 are not sensitive to the choice of ENSO index, indices based on deseasonalised SST anomalies in the Pacific between 5°S–5°N were constructed, with longitude ranges from (160°E–150°W) to (140°W–90°W) with borders translated 10° between regions. The correlation between the PC and each of the SST anomaly indices is greater than 0.9.

3.4 Statistical methods

Most standard formulae for calculating statistical significances make strong assumptions about the data, for example that they are normally distributed. Instead, here the significance is calculated according to "non-parametric" methods which only assume that the data are representative of the population they are drawn from. A permutation method is used when the autocorrelation of the data is found to be negligible [Efron and Tibshirani, 1993; Davison and Hinkley, 1997], which is described in detail for each kind of analysis in section 4. The distribution of the test statistic derived using this method is then used to estimate the probability α that a measurement as large as that observed in the data would be observed under the null hypothesis (the p-value), and then the measurement is said to be significant at the $(1-\alpha)\times 100\%$ level.

The autocorrelation between monthly mean ZMT in consecutive years is generally not signficant at the 95% level, $2/\sqrt{N}$ where N is the number of years [Chatfield, 2004], north of about 60°N in the model, and representing the data by an AR(1) process does not give a large reduction in the size of the residuals. Therefore here the data can be taken to be white noise and permutation methods can be used. The significance for calculations that use ZMT data south of 60°N is not calculated because the time series have a strong quasi-biennial signature which permutation methods do not take into account, so any calculation of significance here by these methods is meaningless. In the ERA-40 data,

the inter-year autocorrelation is more significant, especially in late winter. These data were found to be well represented by an AR(1) process, because higher order autocorrelation coefficients are small and the sum of the squares of the residuals of the AR processes did not decrease substantially for processes of higher order. The statistical method used on these data is explained in detail in section 4.1. The modelled ZMZW and eddy heat flux are found not to be autocorrelated north of about 30°N.

4 Results

Here I firstly consider the dependence of the vortex winds in the Met Office model on the QBO and ENSO assuming their influences act separately in a linear model and compare these results to those found in ERA-40[2] and other modelling studies. I also consider whether evidence for non-stationarity of the QBO influence on the vortex can be found. Finally I show evidence that the QBO and ENSO combine to influence the vortex in a non-linear way, that is their influences do not act independently.

4.1 Linear analysis of the dependence of vortex winds on the QBO and ENSO

4.1.1 Correlation between equatorial wind and vortex temperature

Figure 12 shows the Pearson correlation between zonal mean November–December (ND) and January–February (JF) mean ZMT with 5°S–5°N mean equatorial ZMZW on a given pressure level in ERA-40 and in the model. The equatorial pressure level is chosen to give the greatest correlation between equatorial ZMZW and DJF mean ZMZW at (60°N, 10 hPa) in each case – 44 hPa in ERA-40 and 30 hPa in the model. For individual months November–February, the 30 hPa level always gives the greatest correlation in the model and either the 36 hPa or 44 hPa level gives the greatest correlation in ERA-40. The ZMZW at (60°N, 10 hPa) is commonly used as a measure of vortex strength. The equatorial pressure level that gives the maximum correlation with the high-latitude ZMZW time series does not change if the ZMZW anywhere within the ranges 55–70°N and 5–30 hPa is used. Choosing the level this way is more robust than if high-latitude ZMT data are used to choose the equatorial pressure level. The data at each grid point has a linear trend removed prior to taking a correlation in order to reduce any low-frequency variability – this is not found to substantially affect the results compared to not removing a trend.

Note that since no model perfectly represents the QBO, the polar vortex or planetary wave activity,

[2]Here and hereafter "ERA-40" refers to the combination of ERA-40 and the ECMWF operational analysis up to September 2008.

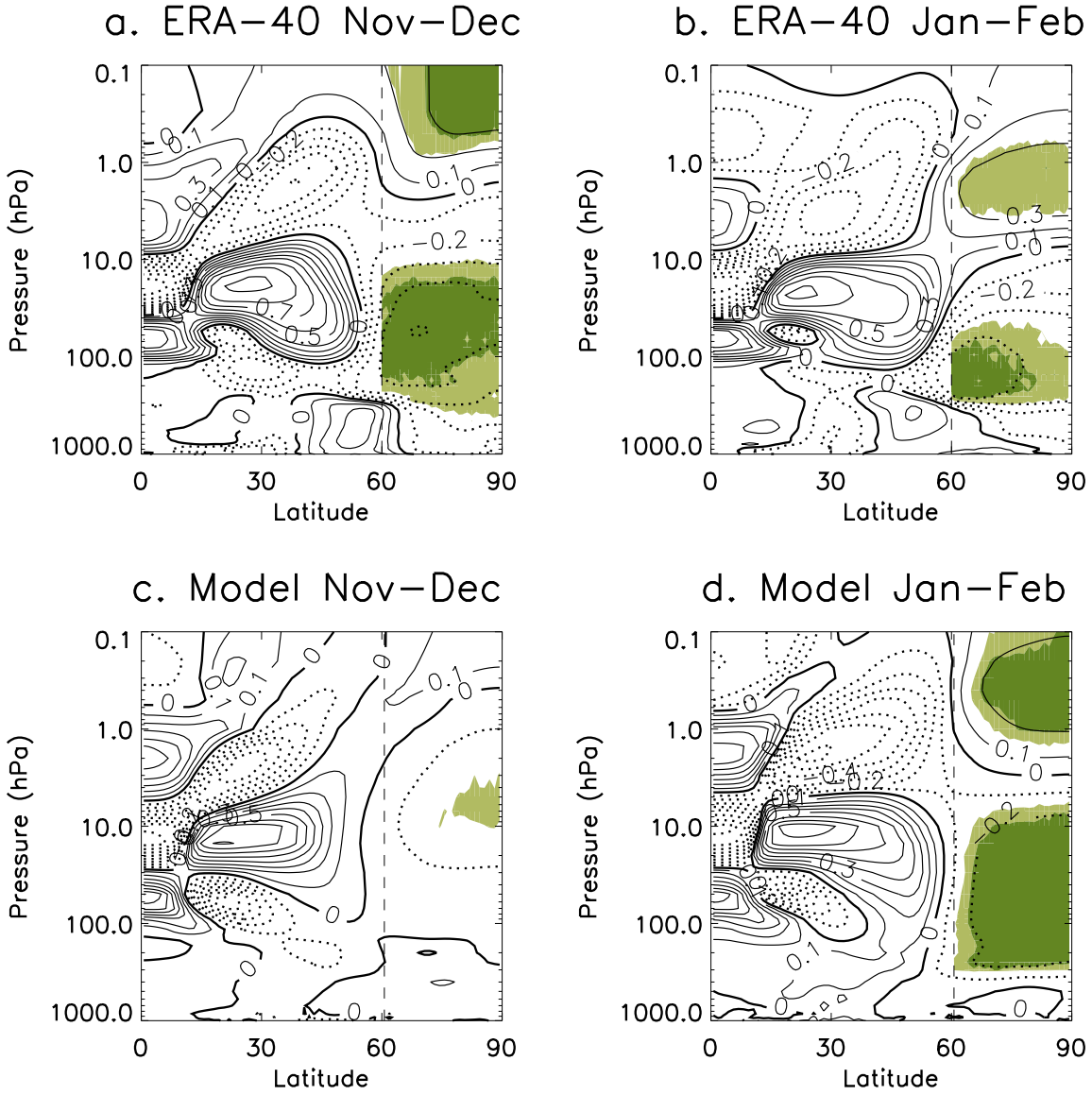

Figure 12: Correlations between Northern Hemisphere zonal mean temperature and 5°S–5°N zonal mean zonal wind in ERA-40 and in the model for November–December and January–February mean winds and temperatures. For ERA-40, equatorial winds at 44 hPa were used and for the model equatorial winds at 30 hPa were used (see text). A linear trend was removed from the temperature and equatorial wind time series. Shading denotes significance at the 95% (light green) and 99% (dark green) levels, calculated north of 60°N. ERA-40 shows a significant negative correlation between polar temperatures and equatorial winds in both periods, whereas the model only captures the relationship in January–February.

it would not be expected that the equatorial level that gives the greatest correlation with high-latitude ZMZW in observations and in a model will perfectly coincide. It is often found in atmospheric models that the equatorial level with the greatest correlation is at a higher altitude than in observations [J. Anstey, pers. comm.]. Also, the large variability of vortex winds means the confidence intervals on correlations with equatorial winds on different pressure levels are large so that it is not possible to be sure which equatorial level would show the largest correlation given an infinitely long set of data. Thus it is not possible to specify *a priori* which level ought to be used to perform correlations and it is appropriate to choose the level that gives the greatest correlation to show the estimated magnitude of the influence of the equatorial winds on the vortex.

Shading in figure 12 denotes statistical significance at the 95% and 99% levels according to a two-tailed test (light and dark green respectively). The equatorial winds are not normally distributed, but rather they are strongly bimodal due to the QBO. Therefore the commonly used assumption that the correlation between two variables is distributed like a t-distribution under the null hypothesis that the populations the data are drawn from are uncorrelated is not valid in this case [Press *et al.*, 1992]. North of 60°N, the model ZMT at each latitude and pressure can be represented by white noise (section 3.4). Thus for testing the significance of the correlations, random permutations of time series of the high-latitude ZMT are generated by assigning a data point chosen at random to each year (without replacement, so each datum is only used once), and leaving the equatorial wind time series unaltered. Then the correlation between each permuted time series and the equatorial wind time series is calculated in order to generate the distribution of the correlation under the null hypothesis. For testing the significance of the ERA-40 ZMT correlation with equatorial wind, where the ZMT data are well represented by an AR(1) process north of 60°N (section 3.4), a similar method was used except that the residuals of the AR(1) process were permuted rather than the data.

In order to check that neglecting inter-year autocorrelation does not significantly affect the results, the significance was also estimated using the phase-shuffling method of Ebisuzaki [2010], which involves randomising the phases of the frequency components of the time series in order to create new time series with the same power spectrum and hence autocorrelation as the original time series, and this gave similar results (not shown). These methods indicated considerably lower statistical significances than did the t-test.

Figure 12(a) shows that in ERA-40, the correlation between ND 44 hPa equatorial ZMZW and ZMT reaches as low as -0.5 north of 60°N, showing the polar vortex between approximately 10–200 hPa is significantly colder when the equatorial winds are westerly compared to when they are easterly.

Correlations with ZMZW (not shown) shows that the polar night jet centred around 60°N is also significantly stronger for more westerly equatorial winds, which is expected given that the monthly mean ZMZW and ZMT are approximately in thermal wind balance. At higher altitudes (above approximately 1 hPa), there is a positive correlation between the equatorial ZMZW and ZMT. This is due to polar mesospheric temperatures being anticorrelated with polar stratospheric temperatures (section 2.1). South of 15°N, the tropical QBO temperature pattern is visible. Between 15–60°N, the pattern of temperature anomalies due to adiabatic warming and cooling associated with the meridional QBO circulation are seen (section 2.2). The ERA-40 JF correlations are less strong and less significant at high latitudes than for ND, reaching as low as -0.4 in the polar stratosphere and upper troposphere (figure 12(b)).

Figure 12(c) shows that the model fails to capture the observed ND correlation between equatorial ZMZW and polar ZMT, but figure 12(d) displays a significant correlation reaching down to approximately -0.3 in the polar stratosphere in JF. Thus the HTR can be studied during this period. This late appearance of the HTR in the model is consistent with the finding that SSWs tend to occur later in the model than in ERA-40 [Osprey *et al.*, 2011]. If the mechanism of the HTR is that the frequency of SSWs is increased during QBO-E, then a model bias towards having too few SSWs in early winter would reduce the size of the correlation between equatorial winds and polar temperatures.

Results for the individual months are similar to those in the 2-month composites in figure 12. No significant correlations between equatorial ZMZW and polar ZMZW or ZMT are found in the month of March in ERA-40 or in the model.

The Pearson correlation may give misleading results if the variables being correlated are not related in a linear way. It was checked that a linear fit to the data was appropriate according to the methods of von Storch and Zwiers [1999]. A scatter plot of polar ZMT against equatorial winds in the model and ERA-40 (not shown) shows a large amount of variability in the ZMT with a lot of overlap between ZMT ranges during QBO-E and QBO-W. This suggests the QBO's influence on the vortex is fairly weak. The data do not indicate any particular equatorial wind magnitude is special and should be used as a cut-off to define QBO-E and QBO-W years, which is a necessary consideration when compositing years in different QBO phases. Thus in section 4.3 the QBO-E and QBO-W phases are just defined according to the sign of the equatorial wind, and robustness of the results against varying the definition of the QBO phases is tested.

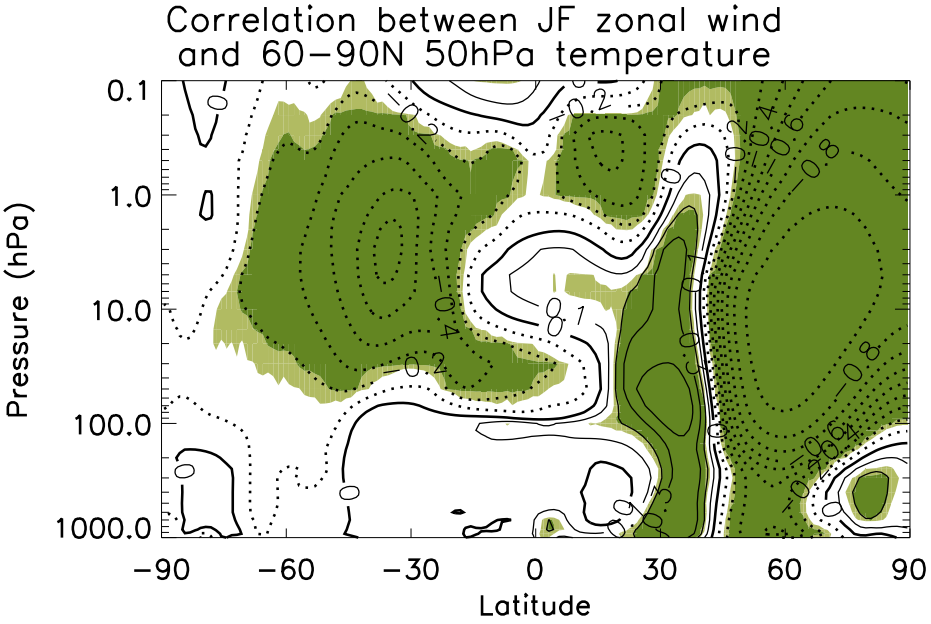

Figure 13: Correlation between January–February zonal mean zonal wind and 60–90°N zonal mean temperature at 50 hPa, with a linear trend removed, in the model. The QBO pattern can be seen at the Equator, although correlations with equatorial winds higher in the stratosphere and in the Southern Hemisphere are greater.

4.1.2 Influence of equatorial upper stratospheric wind on the vortex

Section 2.3.2 explains the evidence for the equatorial upper stratosphere having an important influence on the polar vortex as well as the lower stratospheric winds. In order to see if any evidence for this can be found in the model data, figure 13 shows the correlation of ZMZW with 60–90°N (area-weighted) mean ZMT at 50 hPa (so whereas figure 12 shows the influence of lower stratospheric equatorial ZMZW on ZMT elsewhere, figure 13 shows the influence of ZMZW elsewhere on polar lower stratospheric ZMT, or vice versa).

There is a strong negative correlation between the polar ZMT and ZMZW north of about 50°N in the stratosphere, which is expected from the thermal wind relationship. The QBO pattern of winds is seen at the Equator, but the largest correlation there is about -0.2. There is a stronger correlation with winds in the upper stratosphere, reaching -0.6 near (15°N,0.5 hPa). This is consistent with the view that the upper stratospheric equatorial zonal wind is having a large influence, but it is also possible that the direction of causality is the other way. A warmer, more disturbed vortex is correlated with greater planetary wave activity, which would drive a stronger Brewer-Dobson circulation in the

stratosphere, which would advect easterly stratospheric winds in the SH northwards [L. Gray, pers. comm.]. This would then give a negative correlation between SH and equatorial upper stratospheric winds with polar lower stratospheric temperatures, as shown in the data. This may also explain the strong negative correlation with SH upper stratospheric winds around 40S. Thus the role of this effect needs to be disentangled before these data can be used to support the hypothesis that the equatorial upper stratospheric winds are influencing the vortex.

4.1.3 Multiple linear regression analysis

The straightforward correlation analysis does not take into account the influence of ENSO on the vortex. If the QBO and ENSO indices were correlated or if their effect on the vortex were similar then it would be possible for a correlation analysis to ascribe effects due to ENSO to the QBO or vice versa. Thus the previous results were checked using a multiple linear regression analysis, in which the vortex wind is modelled as a linear function of equatorial winds, ENSO and a trend term plus a random error,

$$u(\mathbf{x},t) = \sum_{i=1}^{4} c_i(\mathbf{x})\chi_i(t) + \epsilon(\mathbf{x},t) \tag{1}$$

where $u(\mathbf{x},t)$ is the zonal mean wind at position $\mathbf{x}$ in the latitude-height plane and time t, $c_i(\mathbf{x})$ is the spatial pattern corresponding to the indices $\chi_i(t)$ and $\epsilon(\mathbf{x},t)$ is the residual.

The equatorial winds are represented by the first two EOFs of the equatorial winds between 5°S–5°N, labelled QBO-A (c_1) and QBO-B (c_2), so there are four terms in the summation. Together these account for 94% of the variance of equatorial lower stratospheric winds [Baldwin and Dunkerton, 1998]. χ_1 and χ_2 are the corresponding principal components. The QBO resembles a travelling wave in equatorial winds that descends with time, and its first two EOFs are spatial patterns that correspond to this wave with a phase difference of a quarter cycle between them. Thus the equatorial winds may be represented approximately as

$$u_{QBO}(\mathbf{x},t) \approx \sum_{i=1}^{2} c'_{i,QBO}(\mathbf{x})\chi'_i(t) \tag{2}$$

where the 'QBO' subscript indicates the spatial domain is taken to be the equatorial lower stratosphere. The primes indicate the spatial patterns and principal components are distinct from those used in the linear regression, but are related by a "rotation". As the spatial patterns $c'_{i,QBO}(\mathbf{x})$ are orthogonal, the equatorial wind state at a given time can be represented as a point in two dimensions, with coordinates ($\chi'_1(t)$,$\chi'_2(t)$). In such a space, the tip of the vector ($\chi'_1(t)$,$\chi'_2(t)$) approximately traces a circle during each QBO cycle, so that the angular position of this vector can be used to define the QBO phase [Wallace *et al.*, 1993]. The basis picked out by the decomposition into EOFs is quite

arbitrary, so in order to produce a more physically meaningful basis, the QBO indices were "rotated" such that $\chi_1 = \cos(\theta)\chi_1' - \sin(\theta)\chi_2'$ and $\chi_2 = \cos(\theta)\chi_2' + \sin(\theta)\chi_1'$, where θ is constant, in order that the regression of $u(60°\text{N}, 10\,\text{hPa}, t)$ onto the QBO-A pattern is maximised and the regression onto the QBO-B pattern is zero. Thus the regression onto QBO-A captures the vortex response and that onto QBO-B captures the ZMZW response associated with the QBO phase when the vortex response is minimal – this information is lost in the previous correlation analysis.

Figure 14 shows the results of the linear regression of NH ZMT against the QBO and ENSO EOF indices for months November–March in the model data. The regression against the linear trend showed nothing significant. Replacing the ENSO EOF index by any of the SST anomaly indices (section 3.3) makes little difference to the results.

The influence of the QBO-A index is found to be similar as for the 30 hPa winds previously, and the regression onto equatorial ZMZW shows a maximum at this level (not shown). The regression also shows the polar upper stratosphere is significantly colder in December for more westerly equatorial winds, which was a considerably less significant signal in the correlation analysis. The QBO-A cold vortex signal descends as the winter advances, lasting into February. The regression of QBO-B onto equatorial ZMZW shows a maximum at ∼10 hPa, and there are significant upper stratospheric cold anomalies for positive values of this index in January–March which descend with time.

It is notable that in both the correlation and regression analyses, the ZMT regression patterns against the equatorial winds in ERA-40 and the model show the mid-latitude QBO meridional circulation pattern and the vortex pattern are approximately vertically aligned between December–February and of opposite sign. This means the meridional temperature gradient is larger than if they were not vertically aligned, which implies a larger vertical wind shear and stronger high-altitude winds by the thermal wind equation. Since the vortex is a non-linear system, feedbacks may occur so that the driving of the vortex to a stronger state in this way may have a relatively large influence later in time. This provides a simple conceptual model of how the QBO meridional circulation may affect the polar vortex.

The regression against the ENSO index shows WENSO significantly warms the vortex in March only, so that its effect is weaker and occurs later in the Met Office model than in observations and in most modelling studies cited in section 2.4. This could be due to WENSO exciting too small a response in planetary wave activity. This signal is well separated from that of the regression against QBO-A, showing little interference between the two vortex forcings according to the linear model (1).

Statistical significance was calculated by forming random permutations of the time series of (60°N, 10 hPa) ZMZW and high-latitude ZMT north of 60°N, in the same way as for the correla-

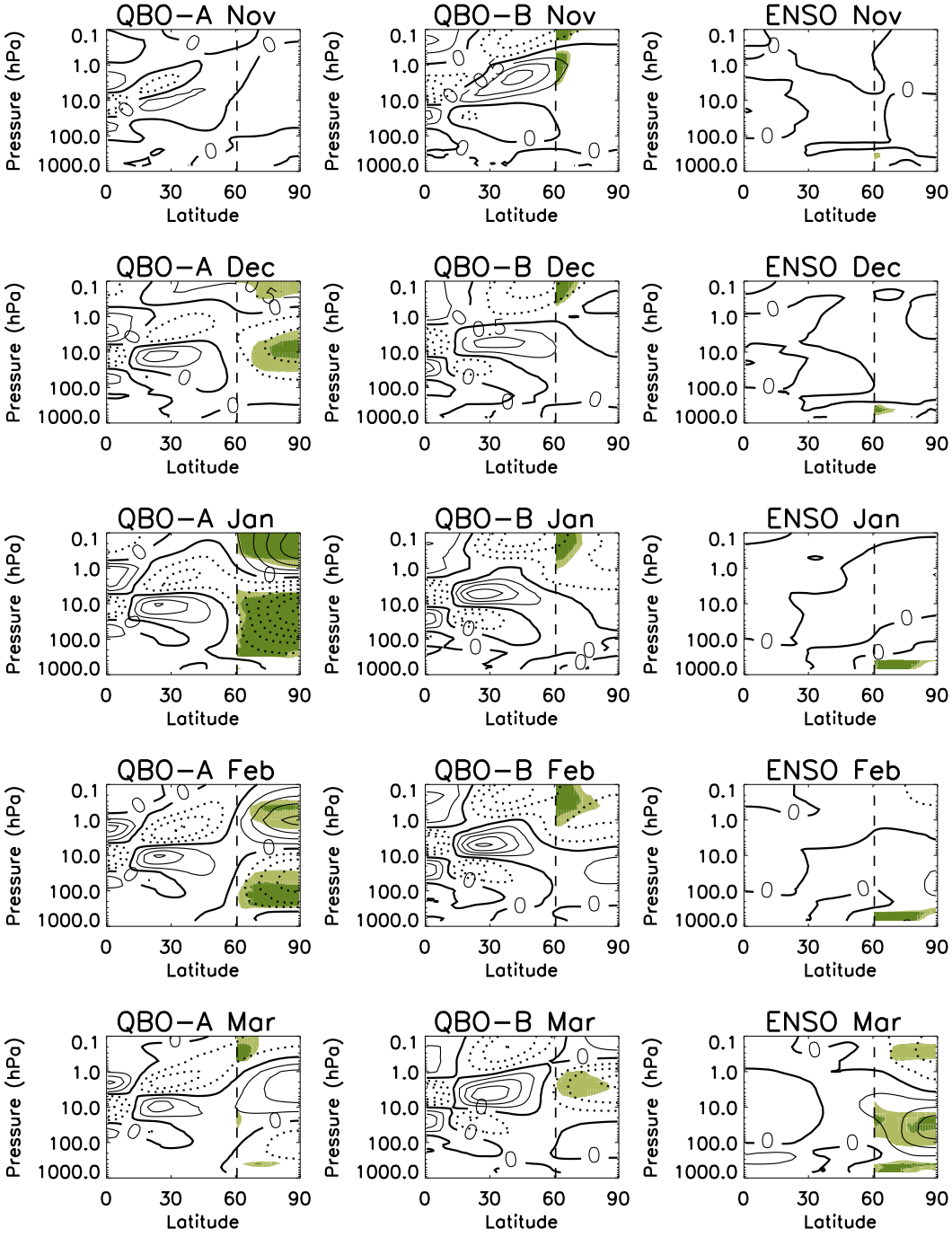

Figure 14: Multiple linear regression of Northern Hemsiphere monthly and zonal mean temperature against QBO-A, QBO-B and ENSO indices (see text) for November–March, showing the change in temperature per one standard deviation change in each of these indices in a linear model. The contour interval is 0.5 K. Shading shows statistical significance at the 95% (light green) and 99% (dark green) levels, calculated north of 60°N, indicated by the vertical dashed line. Produced by adapting code provided by L. Gray. Westerly equatorial winds are associated with colder vortex temperatures in December–February and WENSO with warmer temperatures in March.

tion analysis (with ZMZW and ZMT data for the same year kept together), and performing the same analysis on these random time series as for the model data – the QBO indices were rotated to maximise the random (60°N, 10 hPa) ZMZW and the distribution of regression coefficients at each point of each plot was found so that p-values for the model regression coefficients could be calculated.

4.1.4 Time lag in vortex response to equatorial wind

The above analysis has focussed on the relationship between equatorial winds and polar temperatures at the same time. However, it is possible there could be a significant time lag between variations in equatorial winds affecting the polar vortex, which may be expected to be of the order of the time it takes for planetary waves to propagate from the tropics to high latitudes. The correlation between polar ZMT in winter months and equatorial ZMZW in previous months was calculated in ERA-40 and in the model in order to find out if greater correlations are obtained by introducing a time lag. It was found that the magnitude of the correlation of polar temperatures with equatorial lower stratospheric winds does not change substantially as the time lag increases, but the equatorial level that gives the greatest correlation moves upwards. This is due to the QBO winds forming a coherent downwards moving pattern, so that equatorial winds on a given level at a given time are very highly correlated with winds at higher levels at previous times. Thus it is not possible to establish exactly what phase of the QBO best strengthens the polar vortex by this method of analysis without also knowing the time it takes for the QBO's influence to be felt. This means it is not possible to deduce which equatorial height range is having the greatest influence on the vortex by observations alone. However, the coherence of the QBO's downward propagation also means that the influence can be treated as instantaneous when it is not necessary to know the precise mechanism of the influence on the vortex, but the equatorial level according to which the QBO phase is defined must be chosen empirically.

The correlation between polar stratospheric ZMT and upper stratospheric equatorial ZMZW seen in figure 13 was found to vanish if a time lag is introduced between the ZMZW and ZMT data, further suggesting that the correlation may be due to wave activity at high latitudes influencing the equatorial upper stratosphere, rather than the other way around.

4.1.5 Influence of equatorial vertical wind shear

Gray *et al.* [2001b] found that NP stratospheric ZMT is more strongly correlated with the vertical ZMZW shear $\partial u/\partial z$ at the Equator at an altitude of 50km than with lower stratospheric ZMZW in rocketsonde data. Rigby [2010] found in a stratosphere-mesosphere GCM that introducing vertical

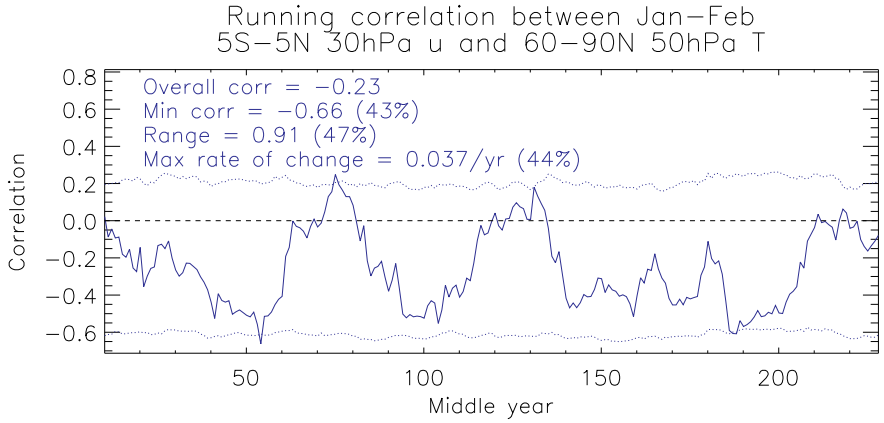

Figure 15: 21-year running correlation between the January–February, 5°S–5°N and zonal mean zonal wind at 30 hPa and January–February, 60–90°N and zonal mean temperature at 50 hPa in the Met Office model (solid line). The dashed lines show the boundaries within which lie 95% of running correlations for random time series of 60–90°N zonal mean temperature generated according to a model in which the polar temperature has a constant linear relationship with the equatorial wind (see text). Also shown are quantitative statistics relating to variations in the running correlation (see text), with the percentage of running correlations for the random temperature time series for which the equivalent statistics exceeded those in the model data in brackets. The model data do not show any greater variability in the correlation than the random time series.

wind shear into an equatorial wind profile increased the frequency of SSWs. The correlation of 60–90°N mean ZMT at 50 hPa with $\partial u/\partial z$ in the Met Office model was calculated to see if this gave an indication of upper stratospheric influence on the polar vortex (not shown). The results resembled simply the vertical derivative of the correlations with ZMZW in figure 13, with the maximum correlations being of similar magnitude in each case. Thus these data do not strongly indicate that the vertical wind shear is playing an important role in the HTR, but also its contribution cannot be ruled out.

4.2 Stationarity of the HTR

Lu *et al.* [2008] suggested that the strength of the HTR varies with time in the ERA-40 re-analysis. Their method was to compute 21-year running correlations between equatorial ZMZW and high-latitude ZMT and ZMZW and show that the correlation varies with time, in a way that is difficult to explain by chance. The running correlation is calculated by computing the correlation in each block of 21 years of consecutive data and assigning that correlation to the mid-point of the block. By plotting time

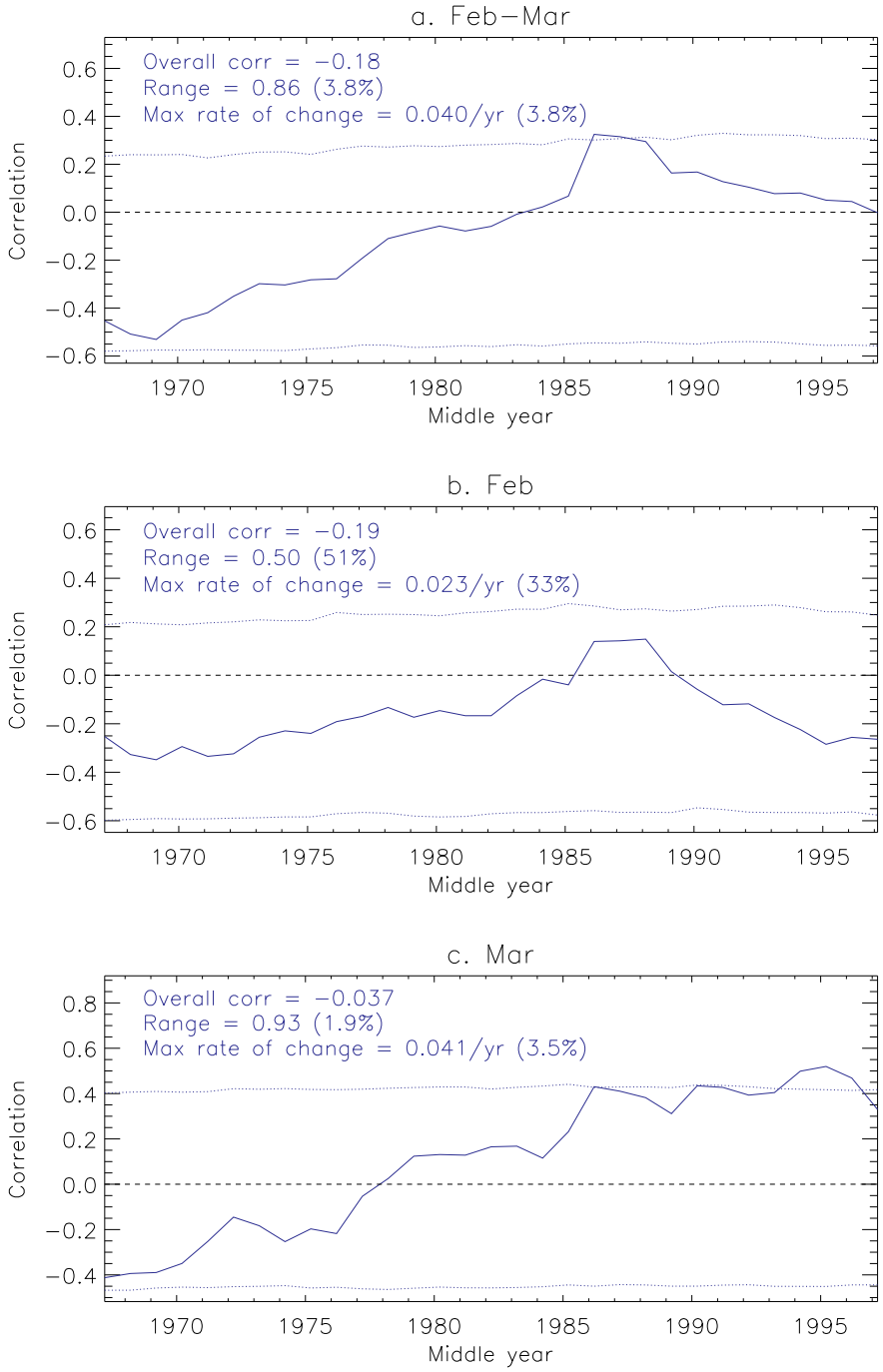

Figure 16: As for figure 15 but for the ERA-40 data, showing the 21-year running correlation between 5°S–5°N zonal mean zonal wind at 44 hPa and 60–90°N zonal mean temperature at 44 hPa, for February–March mean wind and temperature and February and March wind and temperature alone. Only data for the month of March shows significant variation in the running correlation.

series of polar stratospheric ZMT and equatorial stratospheric ZMZW, they found that the correlation appeared to diminish after 1977 and reestablish itself in 1998. They suggested these shifts could be due to either stratospheric ozone depletion and the enhanced greenhouse effect affecting the Brewer-Dobson circulation which then affected the equatorial waveguide for planetary waves, or it may be associated with observed climatic shifts in Pacific SSTs. Other work (see section 2.4) suggests that Pacific SSTs can influence the strength and timing of the HTR. However, Christiansen [2010] suggested it may simply be due to QBO transitions becoming less strongly locked to the seasonal cycle.

In order to see if the model data display variation in the strength of the HTR, figure 15 shows the 21-year running correlation between 5°S–5°N mean ZMZW at 30 hPa and 60–90°N mean ZMT at 50 hPa in the model. The running correlation appears to show considerable variability. To see if these data exclude the null hypothesis that the strength of the HTR is constant, 2000 random ZMT time series were generated according to the model

$$T(t) = \alpha u(t) + \epsilon(t) \tag{3}$$

where the constant α is obtained by a linear fit of the ZMT (T) against the equatorial ZMZW (u) in the model data, and ϵ is a time series of residuals which is shuffled in time to create the random time series. Running correlations with 5°S–5°N mean winds were calculated.

Dotted lines on figure 15 show the boundaries that enclose 95% of these random running correlations. The running correlation for the model data stays mostly within these bounds.

Various quantitative statistics are given in figure 15 and show the behaviour of the model data is not exceptional according to the null hypothesis. These statistics are the minimum correlation, the range of the correlation (the difference between the maximum and minimum) and the maximum rate of change of the running correlation (defined as the gradient of a straight line fitted by the method of least squares to each block of 21 years of consecutive data, 21 years being the minimum resolvable timescale of a 21-year running correlation). The percentages in brackets show the percentage of running correlations for ZMT time series generated according to equation 3 for which the equivalent statistics exceed those in the data. These percentages are all near 50%, showing that variability of the running correlation for the model data is consistent with the dependence of vortex temperatures on equatorial winds being constant in time, as in equation 3. This is also the case for running correlations calculated for a range of block lengths of 15–50 years, for correlations with winds on all equatorial stratospheric levels in all calendar months October–March. Therefore there is not strong evidence that the modelled HTR is non-stationary based on this analysis alone.

Applying this analysis to the ERA-40 data, correlations between equatorial u and polar T averaged over any combination of months between November and February also shows no behaviour inconsistent with the relationship being stationary. However, including March data produces a strong drift in the running correlation, as found by Lu *et al.* [2008]. Figure 16(a) shows the 21-year running correlation between 5°S–5°N ZMZW at 44 hPa and 60–90°N ZMT at 44 hPa obtained for February–March (FM) mean ZMZW and ZMT, figure 16(b) for February data alone and figure 16(c) for March data alone. The FM and March data show a strong drift in the running correlation, with the range and maximum rate of change of the running correlation significant above the 95% level against the null hypothesis that polar ZMT and equatorial ZMZW are related by equation 3. The minimum correlation is not significant for any of the periods and is not shown. The p-value obtained for the range of the running correlation in FM of 3.9% is similar to that obtained by Lu *et al.* [2008] for the running correlation between equatorial ZMZW at 50 hPa and the ZMT at (65°N, 50 hPa) (the only quantitative statistic they reported), who used a slightly different statistical method. The February data alone, however, show no significant drift in the running correlation.

Thus the conclusion that the HTR in observations is non-stationary is sensitive to excluding March from the analysis. Since March is near the end of the winter period when polar stratospheric variability starts decreasing and since there is no significant overall correlation between polar stratospheric ZMT and equatorial stratospheric ZMZW in March, it is not clear that this should be interpreted as a change in the HTR. Also, the p-values for the quantitative statistics measuring the change in the running correlation in FM and March are not very extraordinary, especially considering that five months were examined. Therefore there does not seem to be strong evidence that the observed HTR has varied in strength on decadal time scales.

4.3 Non-linear analysis - the combined influence of the QBO and ENSO on the vortex

The top panel of figure 17 shows the daily and 60–90°N mean ZMT on all pressure levels above 700 hPa as a function of date during the winter, smoothed with an 11-day centred moving average, composited for all winters. The annual cycle is most clearly visible between ∼10–100 hPa where the ZMT changes by ∼20 K, corresponding to the formation and break-up of the vortex. The ZMT reaches a minimum of ∼210 K in December. Winters were assigned to QBO-E and QBO-W composites according to the sign of the monthly and 5°S–5°N mean ZMZW at 30 hPa in November.

The HTR is apparent as a warming of the high-latitude NH stratosphere in QBO-E relative to

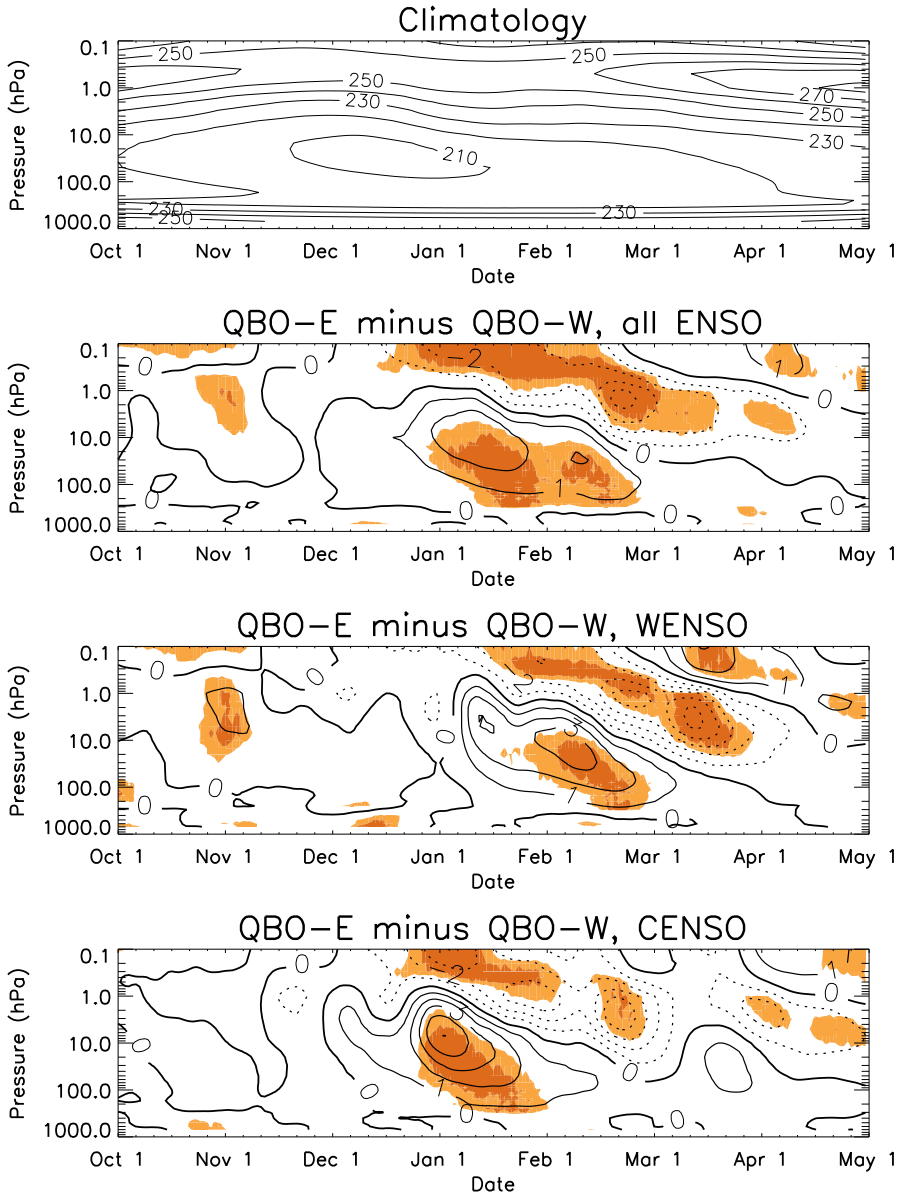

Figure 17: Daily, 60–90°N and zonal mean temperature composites for October–April above 700 hPa showing the climatology for all years (top), then the difference between the QBO-E and QBO-W composites, defined according to the sign of the 5°S–5°N and zonal mean zonal wind at 30 hPa in November (second panel). The third and bottom panels show the difference between the QBO-E and QBO-W composites in only WENSO and CENSO years respectively, with the ENSO phase defined according to the sign of the first PC of tropical Pacific SST in November. Units are K. The data are smoothed with an 11-day centred moving average. Shading denotes statistical significance of the composite differences at the 95% (orange) and 99% (red) levels. The warming of the vortex by QBO-E is advanced during CENSO as compared to WENSO.

QBO-W, displayed in the second panel of figure 17 which shows the difference between the composites for QBO-E and QBO-W winters. The warming begins in late December near 10 hPa and descends with time, peaking at ∼3 K near 10 hPa in mid-January, with the signal remaining significant until late February, consistent with the multiple linear regression analysis (figure 14). This corresponds to the vortex taking more time to warm after December in QBO-W winters on average. A negative ZMT difference is present in the uppermost model layers and descends above the positive ZMT difference, remaining significant until late March and peaking at ∼4 K in late February near 2 hPa. The overall pattern corresponds to the signature of an SSW, indicating that QBO-E is tending to increase the SSW frequency.

The third panel of figure 17 demonstrates the results of repeating this analysis only for WENSO winters, and the bottom panel only for CENSO winters. The ENSO phase has been determined according to the sign of the first PC of tropical Pacific SST in November (section 3.3). As for the equatorial winds, scatter plots of vortex ZMT against ENSO index do not indicate that any particular ENSO index threshold should be used, and so it is preferred here not to use a threshold.

The most notable effect is that the QBO's influence becomes apparent earlier and is intensified during CENSO winters, with the QBO-E minus QBO-W ZMT difference peaking at ∼4 K in early January near 10 hPa, whereas it peaks at ∼3 K in early February in WENSO winters, with another less significant peak in mid-January. The QBO influence is also seen to last for a shorter time than it appeared when no compositing was done according to the phase of ENSO. Hence it can be seen that not taking the ENSO phase into account can misleadingly "smear" the QBO-E minus QBO-W composite difference in time and make it appear that the QBO's influence is smaller in amplitude and longer in duration than is really the case.

These results are not sensitive to the choice of month used to define the QBO and ENSO phases. Applying a threshold on the magnitude of the equatorial winds for defining the QBO phase or of the PC for defining the ENSO phase increases the magnitude of the QBO-E minus QBO-W composite differences and makes the WENSO difference more strongly peaked around early February, so the key result that the difference is apparent earlier under CENSO is not affected. If the SST anomalies in a westerly Pacific region are used to index ENSO rather than the SST PC, the QBO influence appears stronger and it appears weaker if SST anomalies in an easterly region are used.

The statistical significances of the composite differences were computed according to a Monte Carlo permutation test (section 3.4). For each date and pressure level in the figures, two random samples were drawn from the data for all the winters with the selected ENSO phase, with sizes equal to the number

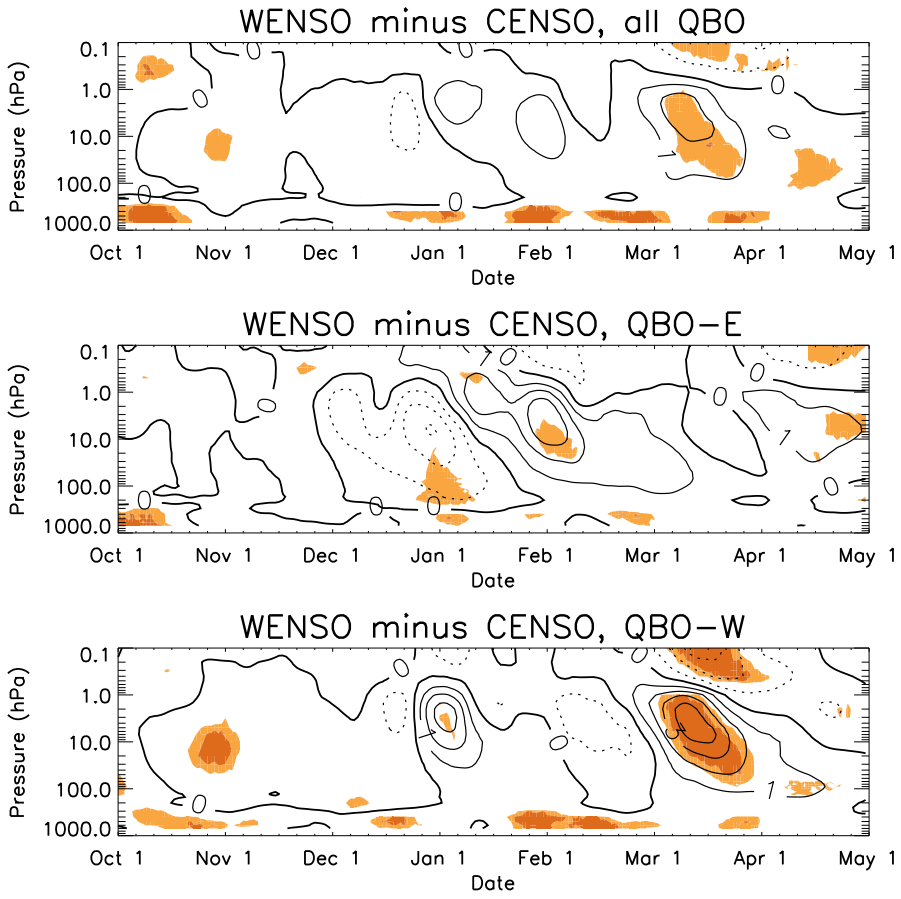

Figure 18: Daily, 60–90°N and zonal mean temperature composites for October–April above 700 hPa showing the difference between the WENSO and CENSO composites, defined according to the sign of the first PC of tropical Pacific SST in November (top). The centre and bottom panels show the difference between the WENSO and CENSO composites in only QBO-E and QBO-W years respectively, with the QBO phase defined according to the sign of the 5°S–5°N and zonal mean zonal wind at 30 hPa in November. Units are K. The data are smoothed with an 11-day centred moving average. Shading denotes statistical significance at the 95% (orange) and 99% (red) levels. The temperature differences are qualitatively different in QBO-E and QBO-W.

of QBO-E and QBO-W winters with that ENSO phase, and the composite difference between these samples computed. This was repeated 1000 times in order to find the probability that the composite difference in the data would be exceeded by chance.

The result that CENSO advances the QBO influence on the vortex relative to WENSO is opposite to that found by Calvo *et al.* [2009]. This could be due to systematic differences between the models

used, as described in section 2.3.2. Their experiment was also different as they used an atmosphere-only model, forced with either climatological or 1997/8 SSTs, the latter corresponding to a strong WENSO event. Thus they lacked a full range of ENSO variability, and it is possible that that event had an anomalous effect on the atmosphere. They also only analysed 26 WENSO winters and it is dubious whether the differences they report are statistically significant (they did not explicitly compute the significance of the differences between their WENSO and climatological SST vortex composites). Comparing these modelling results to observations is very difficult due to the short length of the data record and the influence of other forcings, and has not yet been attempted.

Figure 18 shows the composite daily and 60–90°N mean ZMT differences between WENSO and CENSO above 700 hPa, for both QBO phases and for each phase individually, thus demonstrating the impact of the QBO phase on the vortex response to ENSO. The top panel shows that if no account is taken of the QBO phase, then ENSO only appears to have a significant influence during March, when the vortex is warmer by about 2 K at 10 hPa during WENSO rather than CENSO, which is again consistent with figure 14.

If only QBO-E years are used, however, the vortex is colder by up to 3 K near 10 hPa in late December before becoming warmer by about 2 K in late January. This corresponds to the vortex warming earlier under QBO-E/CENSO than in QBO-E/WENSO in figure 17 (see also figure 21). This has the effect of making the average ZMT anomaly small over the winter, in agreement with observations (section 2.4).

In QBO-W years, the vortex is significantly colder in WENSO compared to CENSO in late October near 10 hPa by just under 1 K. A similar signal was noted by Ineson and Scaife [2009] (who did not separate their model data into different QBO phases), who suggested that this may be due to the wave driving by ENSO interfering destructively with the climatological wave forcing in autumn, so that the vortex is initially made colder during WENSO, in accordance with the ideas of Smith *et al.* [2010]. A negative WENSO minus CENSO ZMT difference in November can also be seen in the modelling and ERA-40 data presented by Manzini *et al.* [2006] and prior to November in the modelling results of Bell *et al.* [2009], and the vortex is less disturbed in October and November in WENSO winters according to the diagnostics of ERA-40 shown by Mitchell *et al.* [2011b]. These were the only other studies cited in section 2.4 to present early winter data.

Ineson and Scaife [2009] found that during winter, the wave driving by WENSO interferes constructively with the climatological forcing, so that the vortex is made warmer. Similarly the vortex is found here to be warmer by up to 3 K between ∼1–10 hPa in early January, although this difference is not highly significant. A much more significant difference of ∼4 K is present descending throughout March

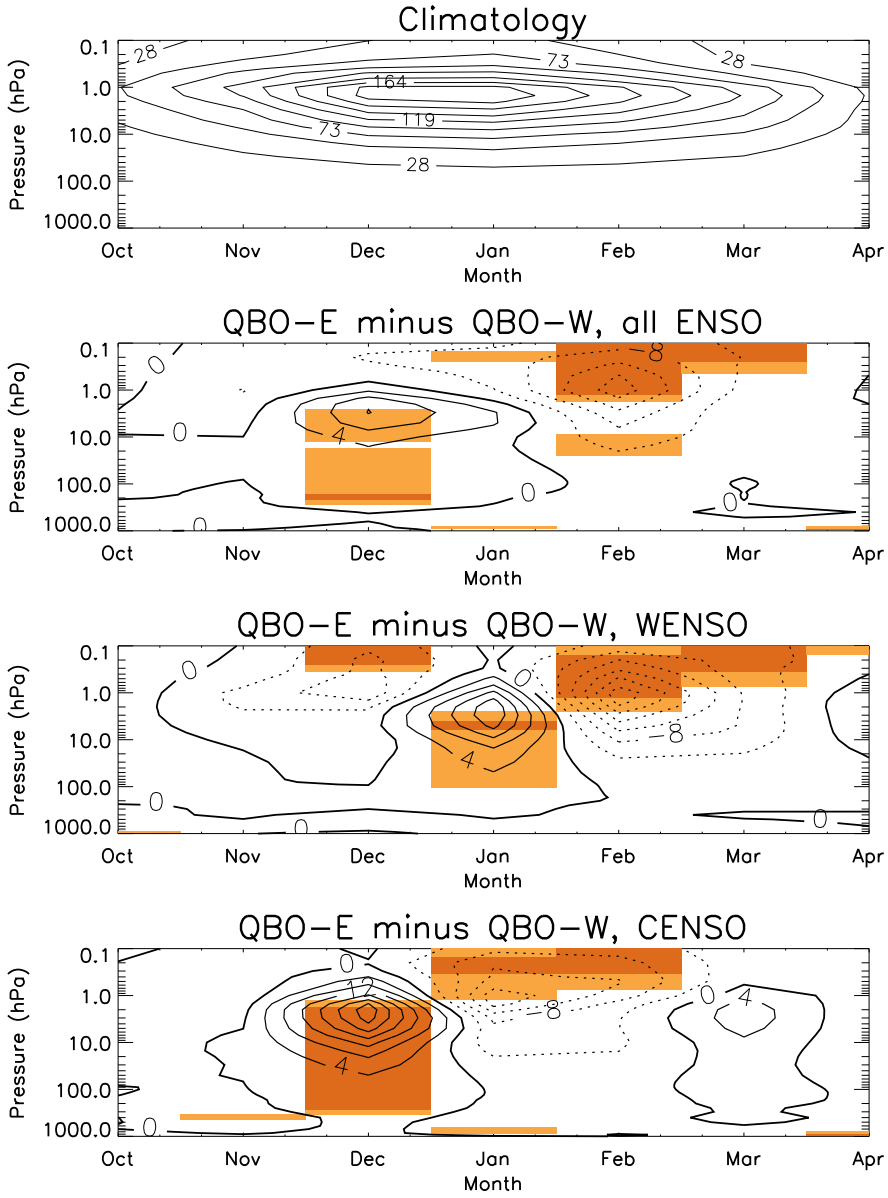

Figure 19: As for figure 17 but for the monthly, 40–80°N and zonal mean $\overline{v'T'}$ between 0.1–1000 hPa. Units are $\mathrm{ms}^{-1}\mathrm{K}$. Significance is indicated by shading a whole month and pressure level where data for that month and pressure level are significant at the 95% (orange) and 99% (red) levels. The enhancement of the wave forcing by QBO-E is advanced during CENSO as compared to WENSO.

with a negative difference above it, corresponding to the SSW signature. These QBO-W differences are made stronger and more significant if a threshold of 0.5 standard deviations is applied to define the ENSO phase, indicating that they are true effects of ENSO and not statistical flukes. The QBO-E differences are not made more significant by applying an ENSO index threshold, however.

Thus it appears that under the QBO-E phase, the main influence of ENSO is on the timing of the vortex warming. Under QBO-W the vortex is initially colder during WENSO compared to CENSO, but is then warmer in middle and late winter. Thus not taking the QBO state into account misses these features of the ENSO influence.

These WENSO minus CENSO composite ZMT differences are fairly robust with regard to changing the compositing month and applying thresholds for defining the QBO and ENSO phases, although for a small number of choices the mid-winter positive ZMT difference under QBO-W is found not to be significant. The composite difference is strongest when the compositing month is taken to be in the concurrent winter rather than the previous winter, contrary to the suggestion of Ren *et al.* [2011]. When no account is taken of the QBO phase, the composite differences are larger and more significant when SST anomalies in an easterly Pacific region are used instead of the SST PC, and the reverse is true for composite differences in separate QBO phases.

The top panel of figure 19 shows the composited monthly, 40–80°N and zonal mean eddy meridional heat flux ($\overline{v'T'}$) for all winters. v' and T' are the deviations of v and T from their zonal means respectively. $\overline{v'T'}$ is proportional to the vertical component of the EP flux and hence is indicative of vertical wave propagation, which may cause easterly acceleration of the flow [Andrews *et al.*, 1987]. The 40–80°N latitude range is used because the largest response of $\overline{v'T'}$ is in this range.

In the second panel of figure 19, the wave activity is seen to be greater in December during QBO-E when not separated according to ENSO and less in February, so it leads the differences in the vortex ZMT in figure 17 by around one month. The third and bottom panels of figure 19 show the composite differences during WENSO and CENSO, which show the enhancement of upward wave flux by QBO-E is advanced in CENSO relative to WENSO, again leading the differences in vortex ZMT by about one month.

Figure 20 shows the composite $\overline{v'T'}$ differences between WENSO and CENSO for both QBO phases and each phase individually. When not separated into QBO-E and QBO-W, there is little significant difference, with a negative difference in October of $\sim$-2.6 $\mathrm{ms^{-1}K}$ at 1 hPa and positive differences in the stratosphere from January onwards. The temperature difference depends on the sum of the difference in wave forcing over the previous months [O'Sullivan and Dunkerton, 1994], so these $\overline{v'T'}$

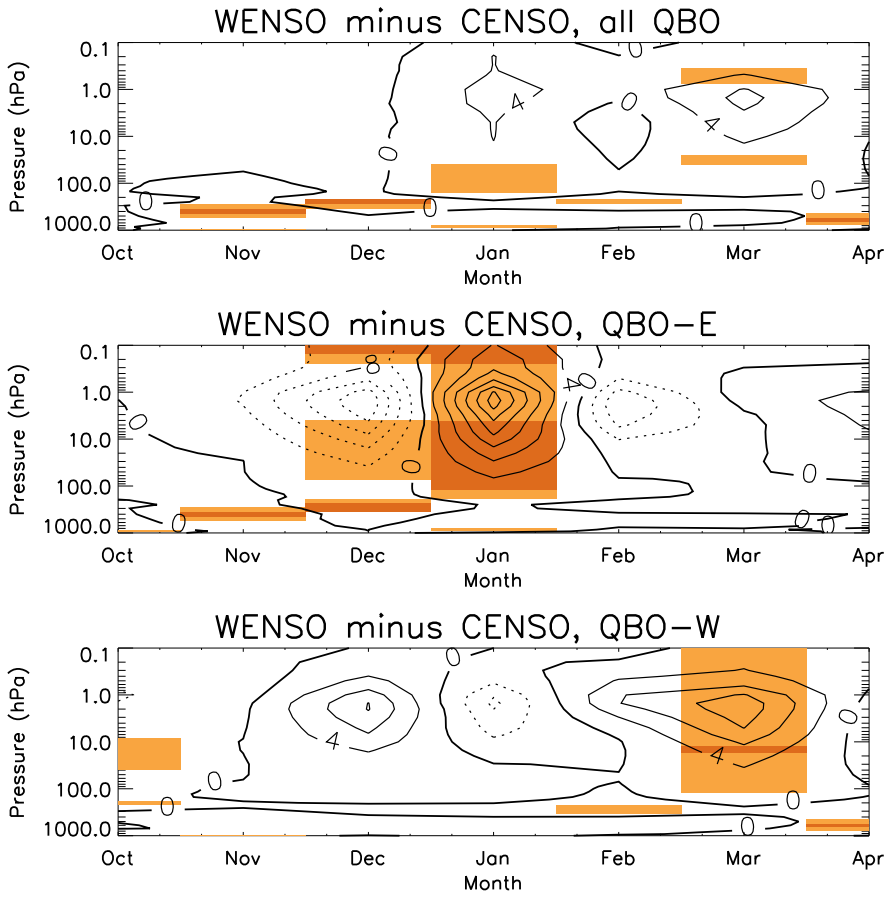

Figure 20: As for figure 18 but for the monthly, 40–80°N and zonal mean $\overline{v'T'}$ between 0.1–1000 hPa. Units are $\mathrm{ms}^{-1}\mathrm{K}$. Significance is indicated by shading a whole month and pressure level where data for that month and pressure level are significant at the 95% (orange) and 99% (red) levels. The wave forcing differences are qualitatively different in QBO-E and QBO-W.

differences eventually give rise to the ZMT difference in March in the top panel of figure 18. Under QBO-E, however, a large negative difference is seen in December and a positive difference in January, corresponding again to CENSO advancing the QBO-E influence. The January positive $\overline{v'T'}$ difference is associated with the transition from a negative ZMT difference in late December to a positive difference in early February near 10 hPa, shown by the middle panel of figure 18. The high significance of this feature indicates that this change in the ZMT difference is also very significant. Under QBO-W, a small negative difference is apparent in October and a large positive difference is not seen until March, which causes the ZMT difference apparent then.

Thus it is seen that the QBO and ENSO are affecting the vortex by influencing at least the vertical

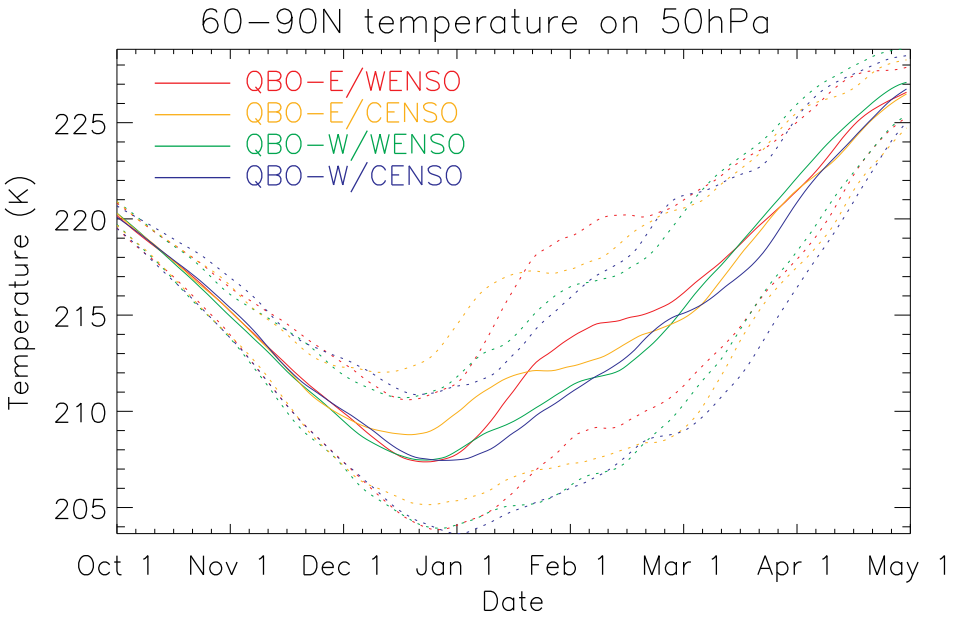

Figure 21: Daily, 60–90°N and zonal mean temperature composites at 50 hPa for QBO-E/WENSO, QBO-E/CENSO, QBO-W/WENSO and QBO-W/CENSO winters, smoothed with an 11-day centred moving average (solid lines). QBO and ENSO phases are defined as in figure 17. Dashed lines show plus/minus one standard deviation.

component of planetary wave flux into the stratosphere.

A question that arises is whether these model data are consistent with the ideas presented in sections 2.3.2 and 2.4 regarding planetary wave forcing needing to be within a particular range for the QBO and ENSO to have an influence on the vortex and winters with QBO-W and CENSO displaying a "least perturbed state" of the vortex.

Figure 21 shows the composite daily and 60–90°N mean ZMT at 50 hPa for QBO-E/WENSO, QBO-E/CENSO, QBO-W/WENSO and QBO-W/CENSO winters. QBO-W/CENSO has the coldest composite ZMT in January and March. QBO-W/WENSO is less distinct from QBO-W/CENSO than are the QBO-E composites, showing that WENSO is less able to warm the vortex than QBO-E. Overall, the picture is fairly consistent with QBO-W/CENSO giving the least disturbed vortex in January and March and with QBO-E and WENSO acting to disturb the vortex, with QBO-E being more effective. However, the timings of when the vortex warms also differ between the different ENSO and QBO phases, occurring earliest for QBO-E/CENSO, which is not explained by WENSO simply acting to disturb the vortex.

5 Discussion and conclusions

This report has examined the influence of the QBO and ENSO on the winter NH stratospheric polar vortex in observations and in the Met Office coupled ocean-troposphere-stratosphere GCM HadGEM2-CCS. The most significant finding is that the QBO and ENSO combine in a non-linear way in the model. The model does not capture the early winter influence of the QBO on the vortex, but it is found that the vortex is warmer when equatorial 30 hPa winds are easterly in late December and January under CENSO and in late January and February under WENSO relative to when the winds are westerly. WENSO seems to have a warming effect on the vortex in late winter during QBO-W, but its main effect actually seems to be on the timing of the QBO-E influence. Hence the QBO and ENSO do not have well-defined independent influences on the vortex and ought to be considered in combination for the model data.

As well as being dynamically interesting, this has implications for determining the effects of the QBO and ENSO on the vortex in observations. Studies have typically considered the QBO and ENSO influences on the vortex separately, which for these model results would lead to the impression that the magnitude of these influences is less than in reality. This may in turn lead to the utility of the QBO and ENSO for seasonal forecasting of vortex variability and NH weather to be underestimated. No evidence was found for the HTR to be non-stationary on decadal time scales, but these results imply that the influence of the QBO on the vortex does vary with the phase of ENSO, on time scales of several years.

A tentative explanation for the finding that CENSO advances the timing of the warming under QBO-E relative to WENSO is that under WENSO conditions, the vortex is colder in late October and early November (figure 18). This indicates that CENSO may be preconditioning the vortex [McIntyre, 1982; Charlton and Polvani, 2007] to be more prone to SSWs occurring early in the winter, so SSWs occur earlier under QBO-E/CENSO than under QBO-E/WENSO. Relative to the influence of QBO-E, the wave forcing provided by WENSO is small, so its warming influence is not apparent under QBO-E. Under QBO-W, vortex warming occurs later (figure 21), so the effect of WENSO suppressing early winter disturbances is not apparent, and late winter warming by WENSO is seen once the additional wave forcing has had its effect. This would imply that the timing of the WENSO event is important.

This suggests the simple conceptual model presented in figures 8 and 9 does not capture all the aspects of the response of the vortex to the QBO and ENSO, as the perturbation by each to the effective wave forcing may vary as winter progresses, so that not just the magnitude of the vortex disturbance is affected but also the timing of when the disturbance occurs. The mean response of the

vortex in a given QBO/ENSO phase cannot be completely represented by something like a seasonal average.

In order to understand how the QBO and ENSO are combining to influence the vortex, further analysis on the model data I have been using can be carried out. Firstly, the wave activity in the model can be examined in more detail, for example by analysing the EP flux in the different QBO and ENSO phases in order to understand how the supposed increased poleward stratospheric flux under QBO-E and the increased flux into the stratosphere under WENSO are combining to influence the vortex. GPH anomalies can also be studied in order to understand how the QBO and ENSO are affecting the long wavelength components of GPH that may propagate into the stratosphere. It may also be worthwhile to try using the geometrical diagnostics found by Mitchell *et al.* [2011a] to characterise the vortex state more effectively than the ZMZW and ZMT – for example, these diagnostics have more success at picking out major vortex disturbances and distinguishing between vortex displacements and splits. The differences in the frequency and timing of SSWs in the different QBO and ENSO phases could be examined to see how much of the temperature differences is due to large vortex disturbances. The differences between the synoptic evolution of warmings in different QBO and ENSO phases could also be studied, in the same way as by Gray *et al.* [2001a] and Rigby [2010]. Checking these modelling results against observations would help to show if the model is behaving realistically, although obtaining a robust signal is likely to be challenging.

A possible complication arises from the influence of Eurasian snow cover on the vortex in the model. Eurasian snow cover may in principle interact non-linearly with both the QBO and ENSO, which could mean the above analysis of the combined QBO-ENSO influence on the vortex is in error, in the same way that considering the QBO and ENSO as separate influences on the vortex gives a misleading picture of their effects. However, both ENSO and Eurasian snow cover have been found to affect the vortex through producing tropospheric planetary wave anomalies that interfere *linearly* with the climatological wave structure, which affects the stratospheric wave forcing [Smith *et al.*, 2010; Fletcher and Kushner, 2011]. This implies that Eurasian snow cover does not interfere non-linearly with the ENSO influence on the vortex and may act effectively as a noise term. The magnitude of the effect of snow cover is also currently uncertain [J. Anstey, pers. comm.]. It should, however, be verified that there are no significant differences between the QBO-ENSO influence in years with different levels of snow cover.

6 Future work

The further analysis of the Met Office model data previously described would take an estimated two–three months to complete. Beyond that, it is proposed to carry out further model runs in order to better understand and characterise the way the QBO and ENSO influence the vortex, controlling ENSO variability and exploring how the influence varies as the ENSO state is changed.

A proposed set of experiments is as follows. Following Bell *et al.* [2009], who investigated the impact of ENSO on European winter climate in a different GCM, the model could be run in its atmosphere-only configuration with imposed SSTs, which would be observed climatological SSTs and a set of different ENSO states. A "typical" WENSO SST pattern could be produced by compositing several similar ENSO events in observations – Bell *et al.* [2009] used average SST anomalies in the winters 1982/3, 1986/7, 1991/2 and 1997/8 in the region 5°S–5°N and 140°E–100°W. Alternatively the first EOF of tropical Pacific SSTs could be used. Then different ENSO SST patterns would be produced by adding or subtracting one or two times this typical WENSO anomaly from the climatological SSTs, to give five SST patterns in total. Then differences in the vortex state between the QBO phases for each ENSO state, and between the ENSO states for each QBO phase, could be examined in order to understand how the vortex state depends on both of these influences. ENSO variability would be controlled better than in the results presented in this report and a greater range of ENSO states would be sampled. Additional experiments could be aimed at investigating the role of the timing of ENSO on the vortex, in order to test the hypothesis in section 5.

Based on the fact that 240 years of model data were required to just about see the difference between WENSO and CENSO vortex ZMT in the two different QBO phases, I would anticipate that about 100 years of data would be required for each SST pattern in order to see a significant difference between the different ENSO phases, requiring 500 years of data in total. However, as ENSO variability is controlled, the interannual vortex variability could be smaller. Also, the ENSO SST anomalies that would be used are stronger than typical anomalies, so any signal should be correspondingly larger. Therefore it may be the case that fewer model years would be required to get a significant signal.

A test run of HadGEM2-CCS on the Hector supercomputing system found that producing one model month of data took 1h 45min. Using fixed SSTs and removing the carbon cycle could speed the model up by a factor of $\sim$2 [S. Osprey, pers. comm.], meaning 500 years of model data would take about seven months of computer time to produce. Four jobs may be run in parallel, so that the data could be produced in two–three months, allowing for queueing time, and it is intended to begin this work in September 2011.

The QBO influence on the vortex has been found to be large in this report. The Met Office model produces a realistic QBO such that the distribution of equatorial winds is strongly bimodal, as in observations. Artificially modifying the QBO state in the model, for example by relaxing to a prescribed equatorial ZMZW, would disrupt the model physics and possibly induce unrealistic features into the circulation [L. Gray, pers. comm.]. Therefore I don't consider it necessary or desirable to investigate the effect of varying the equatorial winds on the vortex state in the same way as investigating the ENSO influence above.

It may then be feasible to have the proposed model runs completed by about the end of 2011, and the analysis completed by the end of the second year of my studies. There are two foreseeable ways this work could be extended into my third year. One would be to examine the impact of the QBO and ENSO on European winter climate. Several studies have found that WENSO events are connected to a more negative NAO index in late northern winter [van Loon and Madden, 1981; Mathieu *et al.*, 2004; Brönnimann *et al.*, 2004, 2006; Brönnimann, 2007], and that the mechanism involves disruption of the vortex [Ineson and Scaife, 2009; Bell *et al.*, 2009; Cagnazzo and Manzini, 2009]. Since this report has shown that the impact of ENSO on the vortex is modulated by the QBO, this may mean that there is a corresponding signal in European winter climate. Use of the Met Office model would allow detailed study of the mechanism of this teleconnection.

A second potential avenue of study would be to investigate the combined role of the QBO, ENSO and the solar cycle on the vortex. An interaction between the solar cycle and the QBO in influencing the vortex has previously been proposed from observational and modelling work [Labitzke, 1987, 2005; Camp and Tung, 2007b]. Thus it may be suspected that ENSO could combine non-linearly with both these influences to affect the vortex. D. Mitchell is currently running the Met Office model with only natural forcings, which would provide data free from anthropogenic influences which would allow the impact of these influences on the vortex to be studied. The total run time would be ∼500 years, which would be sufficient to detect non-linear influences of the solar cycle if they are of similar magnitude to the QBO and ENSO influences. These runs are expected to be completed in early 2012.

Acknowledgements: I am of course very grateful to my supervisors Lesley Gray and David Andrews for their help and guidance in the past year. I also wish to thank Scott Osprey, Daniel Mitchell and James Anstey for many helpful discussions.

References

Allen R, Zender C. 2010. Effects of continental-scale snow albedo anomalies on the wintertime Arctic oscillation. *J. Geophys. Res.* **115**: D23105, doi:10.1029/2010JD014490.

Ambaum M, Hoskins B. 2002. The NAO troposphere-stratosphere connection. *J. Climate* **15**(14): 1969–1978.

Andrews D, Holton J, Leovy C. 1987. *Middle atmosphere dynamics*. Academic Press.

Anstey J, Shepherd T, Scinocca J. 2010. Influence of the quasi-biennial oscillation on the extratropical winter stratosphere in an atmospheric general circulation model and in reanalysis data. *J. Atmos. Sci.* **67**(5): 1402–1419.

Baldwin M. 2003. Comment on "Tropospheric response to stratospheric perturbations in a relatively simple general circulation model" by Lorenzo M. Polvani and Paul J. Kushner. *Geophys. Res. Lett.* **30**(15), doi:10.1029/2003GL017793.

Baldwin M, Dunkerton T. 1991. Quasi-biennial oscillation above 10 mb. *Geophys. Res. Lett.* **18**: 1205–1208.

Baldwin M, Dunkerton T. 1998. Quasi-biennial modulation of the Southern Hemisphere stratospheric polar vortex. *Geophys. Res. Lett.* **25**: 3343–3346.

Baldwin M, Dunkerton T. 1999. Propagation of the Arctic oscillation from the stratosphere to the troposphere. *J. Geophys. Res.* **104**: 30 937–30 946.

Baldwin M, Dunkerton T. 2001. Stratospheric harbingers of anomalous weather regimes. *Science* **294**: 581–584.

Baldwin M, Gray L. 2005. Tropical stratospheric zonal winds in ECMWF ERA-40 reanalysis, rocketsonde data, and rawinsonde data. *Geophys. Res. Lett.* **32**(9): L09806, doi:10.1029/2004GL022328.

Baldwin M, Gray L, Dunkerton T, Hamilton K, Haynes P, Randel W, Holton J, Alexander M, Hirota I, Horinouchi T, *et al.* 2001. The quasi-biennial oscillation. *Rev. Geophys.* **39**(2): 179–229.

Baldwin M, O'Sullivan D. 1995. Stratospheric effects of ENSO-related tropospheric circulation anomalies. *J. Climate* **8**(4): 649–667.

Baldwin M, Stephenson D, Thompson D, Dunkerton T, Charlton A, O'Neill A. 2003a. Stratospheric memory and skill of extended-range weather forecasts. *Science* **301**(5633): 636–640.

Baldwin MP, Thompson DWJ, Shuckburgh EF, Norton WA, Gillett NP. 2003b. Weather from the stratosphere? *Science* **301**(5631): 317–319.

Bell C, Gray L, Charlton-Perez A, Joshi M, Scaife A. 2009. Stratospheric communication of El Niño teleconnections to European winter. *J. Climate* **22**: 4083–4096.

Brönnimann S. 2007. Impact of El Niño–Southern Oscillation on European climate. *Rev. Geophys.* **45**(3).

Brönnimann S, Luterbacher J, Staehelin J, Svendby T, Hansen G, Svenoe T. 2004. Extreme climate of the global troposphere and stratosphere in 1940–42 related to El Niño. *Nature* **431**(7011): 971–974.

Brönnimann S, Schraner M, Mueller B, Fischer A, Brunner D, Rozanov E, Egorova T. 2006. The 1986-1989 ENSO cycle in a chemical climate model. *Atmospheric Chemistry and Physics* **6**: 4669–4685.

Butler A, Polvani L. 2011. El Niño, La Niña, and stratospheric sudden warmings: A reevaluation in light of the observational record. *Geophys. Res. Lett.* **38**(13): L13807, doi:10.1029/2011GL048084.

Cagnazzo C, Manzini E. 2009. Impact of the stratosphere on the winter tropospheric teleconnections between ENSO and the North Atlantic and European region. *J. Climate* **22**(5): 1223–1238.

Calvo N, García-Herrera R, Garcia R. 2008. The ENSO signal in the stratosphere. *Annals of the New York Academy of Sciences* **1146**(1): 16–31.

Calvo N, Giorgetta M, Garcia-Herrera R, Manzini E. 2009. Nonlinearity of the combined warm ENSO and QBO effects on the Northern Hemisphere polar vortex in MAECHAM5 simulations. *J. Geophys. Res.* **114**(D13): D13109, doi:10.1029/2008JD011445.

Calvo N, Giorgetta M, Peña Ortiz C. 2007. Sensitivity of the boreal winter circulation in the middle atmosphere to the quasi-biennial oscillation in MAECHAM5 simulations. *J. Geophys. Res.* **112**: D10124, doi:10.1029/2006JD007844.

Camp C, Tung K. 2007a. Stratospheric polar warming by ENSO in winter: A statistical study. *Geophys. Res. Lett.* **34**(4): L04809, doi:10.1029/2006GL028521.

Camp C, Tung K. 2007b. The influence of the solar cycle and QBO on the late-winter stratospheric polar vortex. *J. Atmos. Sci.* **64**(4): 1267–1283.

Cane MA. 2005. The evolution of El Niño, past and future. *Earth and Planetary Science Letters* **230**(3-4): 227–240.

Chan C, Plumb R. 2009. The response to stratospheric forcing and its dependence on the state of the troposphere. *J. Atmos. Sci.* **66**(7): 2107–2115.

Charlton A, O'Neill A, Lahoz W, Massacand A. 2004. Sensitivity of tropospheric forecasts to stratospheric initial conditions. *Q. J. R. Meteorol. Soc.* **130**(600): 1771–1792.

Charlton A, O'Neill A, Stephenson D, Lahoz W, Baldwin M. 2003. Can knowledge of the state of the stratosphere be used to improve statistical forecasts of the troposphere? *Q. J. R. Meteorol. Soc.* **129**(595): 3205–3224.

Charlton A, Polvani L. 2007. A new look at stratospheric sudden warmings. Part I: Climatology and modeling benchmarks. *J. Climate* **20**: 449–469.

Charney J, Drazin P. 1961. Propagation of planetary-scale disturbances from the lower into the upper atmosphere. *J. Geophys. Res.* **66**(1): 83–109.

Chatfield C. 2004. *The Analysis of Time Series: An Introduction*. Chapman & Hall: London, 6 edn.

Chen W, Takahashi M, Graf H. 2003. Interannual variations of stationary planetary wave activity in the northern winter troposphere and stratosphere and their relations to NAM and SST. *J. Geophys. Res.* **108**(D24): 4797, doi:10.1029/2003JD003834.

Christiansen B. 2010. Stratospheric bimodality: Can the equatorial QBO explain the regime behavior of the NH winter vortex? *J. Climate* **23**(14): 3953–3966.

Cohen J, Barlow M, Kushner PJ, Saito K. 2007. Stratosphere-troposphere coupling and links with Eurasian land surface variability. *J. Climate* **20**(21): 5335–5343, doi:10.1175/2007JCLI1725.1.

Collins WJ, Bellouin N, Doutriaux-Boucher M, Gedney N, Hinton T, Jones C, Liddicoat S, G Martin FO, Rae J, Senior C, Totterdell I, Reichler SWT, Kim J, Halloran P. 2008. Evaluation of the HadGEM2 model. Hadley Centre Technical Note No. 74.

Coughlin K, Gray L. 2009. A continuum of sudden stratospheric warmings. *J. Atmos. Sci.* **66**: 531–540.

Crooks S, Gray L. 2005. Characterization of the 11-year solar signal using a multiple regression analysis of the ERA-40 dataset. *J. Climate* **18**(7): 996–1015.

Davison AC, Hinkley DV. 1997. *Bootstrap methods and their applications*. Cambridge University Press: Cambridge.

Dunkerton T. 1997. The role of gravity waves in the quasi-biennial oscillation. *J. Geophys. Res.* **102**(D22): 26 053–26 076.

Dunkerton T, Baldwin M. 1991. Quasi-biennial modulation of planetary-wave fluxes in the Northern Hemisphere winter. *J. Atmos. Sci.* **48**(8): 1043–1061.

Ebisuzaki W. 2010. A method to estimate the statistical significance of a correlation when the data are serially correlated. *J. Climate* **10**(9): 2147–2153.

Efron B, Tibshirani RJ. 1993. *An introduction to the bootstrap*. Chapman and Hall: New York.

Fernández N, Herrera R, Puyol D, MartÍn E, GarcÍa R, Presa L, RodrÍguez P. 2004. Analysis of the ENSO signal in tropospheric and stratospheric temperatures observed by MSU, 1979–2000. *J. Climate* **17**: 3934–3946.

Fischer AM, Shindell DT, Winter B, Bourqui MS, Faluvegi G, Rozanov E, Schraner M, Broennimann S. 2008. Stratospheric winter climate response to ENSO in three chemistry-climate models. *Geophys. Res. Lett.* **35**(13), doi:10.1029/2008GL034289.

Fletcher CG, Kushner PJ. 2011. The role of linear interference in the annular mode response to tropical SST forcing. *J. Climate* **24**(3): 778–794, doi:10.1175/2010JCLI3735.1.

Free M, Seidel D. 2009. Observed El Niño–Southern Oscillation temperature signal in the stratosphere. *J. Geophys. Res.* **114**: D23108, doi:10.1029/2009JD012420.

Garcia-Herrera R, Calvo N, Garcia R, Giorgetta M. 2006. Propagation of ENSO temperature signals into the middle atmosphere: A comparison of two general circulation models and ERA-40 reanalysis data. *J. Geophys. Res.* **111**: D06101, doi:10.1029/2005JD006061.

Garfinkel C, Hartmann D. 2007. The effects of the quasi-biennial oscillation and the El Nino Southern Oscillation on polar temperatures in the stratosphere. *J. Geophys. Res.* **112**: D19112, doi:10.1029/2007JD008481.

Garfinkel C, Hartmann D. 2008. Different ENSO teleconnections and their effects on the stratospheric polar vortex. *J. Geophys. Res.* **113**: D18114, doi:10.1029/2008JD009920.

Garfinkel C, Hartmann D. 2010. Influence of the quasi-biennial oscillation on the North Pacific and El Niño teleconnections. *J. Geophys. Res.* **115**: D20116, doi:10.1029/2010JD014181.

Garfinkel C, Hartmann D, Sassi F. 2010. Tropospheric precursors of anomalous Northern Hemisphere stratospheric polar vortices. *J. Climate* **23**(12): 3282–3299.

Garfinkel C, Shaw T, Hartmann D, Waugh D. 2011. Does the Holton-Tan mechanism explain how the quasi-biennial oscillation modulates the Arctic polar vortex? *J. Atmos. Sci.* Submitted.

Gray L. 2003. The influence of the equatorial upper stratosphere on stratospheric sudden warmings. *Geophys. Res. Lett.* **30**(4): 1166, doi:10.1029/2002GL016430.

Gray L, Crooks S, Pascoe C, Sparrow S, Palmer M. 2004. Solar and QBO influences on the timing of stratospheric sudden warmings. *J. Atmos. Sci.* **61**(23): 2777–2796.

Gray L, Drysdale E, Lawrence B, Dunkerton T. 2001a. Model studies of the interannual variability of the northern-hemisphere stratospheric winter circulation: The role of the quasi-biennial oscillation. *Q. J. R. Meteorol. Soc.* **127**(574): 1413–1432.

Gray L, Phipps S, Dunkerton T, Baldwin M, Drysdale E, Allen M. 2001b. A data study of the influence of the equatorial upper stratosphere on northern-hemisphere stratospheric sudden warmings. *Q. J. R. Meteorol. Soc.* **127**(576): 1985–2003.

Gray L, Sparrow S, Juckes M, O'Neill A, Andrews D. 2003. Flow regimes in the winter stratosphere of the Northern Hemisphere. *Q. J. R. Meteorol. Soc.* **129**(589): 925–945.

Hamilton K. 1989. Interhemispheric asymmetry and annual synchronization of the ozone quasi- biennial oscillation. *J. Atmos. Sci.* **46**(7): 1019–1025.

Hamilton K. 1993a. An examination of observed Southern Oscillation effects in the Northern Hemisphere stratosphere. *J. Atmos. Sci.* **50**(20).

Hamilton K. 1993b. A general circulation model simulation of El Niño effects in the extratropical Northern Hemisphere stratosphere. *Geophys. Res. Lett.* **20**(17): 1803–1806.

Hamilton K. 1998. Effects of an imposed quasi-biennial oscillation in a comprehensive troposphere-stratosphere-mesosphere general circulation model. *J. Atmos. Sci.* **55**(14): 2393–2418.

Hannachi A, Mitchell D, Gray L, Charlton-Perez A. 2011. On the use of geometric moments to examine the continuum of sudden stratospheric warmings. *J. Atmos. Sci.* **68**(3): 657–674, doi: 10.1175/2010JAS3585.1.

Hardiman S, Butchart N, Hinton T, Osprey S, Gray L. 2011. Simulations for CMIP5 run with high and low top versions of the Met Office climate model: Effect of adding a well resolved stratosphere on surface climate. *J. Climate* Submitted.

Harvey V, Hitchman M. 1996. A climatology of the Aleutian high. *J. Atmos. Sci.* **53**: 2088–2102.

Hasebe F. 1994. Quasi-biennial oscillations of ozone and diabatic circulation in the equatorial stratosphere. *J. Atmos. Sci.* **51**(5): 729–745.

Holton J, Austin J. 1991. The influence of the equatorial QBO on sudden stratospheric warmings. *J. Atmos. Sci.* **48**(4): 607–618.

Holton J, Lindzen R. 1972. An updated theory for the quasi-biennial cycle of the tropical stratosphere. *J. Atmos. Sci.* **29**(6): 1076–1080.

Holton J, Tan H. 1980. The influence of the equatorial quasi-biennial oscillation on the global circulation at 50 mb. *J. Atmos. Sci.* **37**(10): 2200–2208.

Holton J, Tan H. 1982. The quasi-biennial oscillation in the Northern Hemisphere lower stratosphere. *Meteorological Society of Japan, Journal* **60**: 140–148.

Hurwitz MM, Newman PA, Oman LD, Molod AM. 2011. Response of the Antarctic stratosphere to two types of El Niño events. *J. Atmos. Sci.* **68**(4): 812–822, doi:10.1175/2011JAS3606.1.

Ineson S, Scaife A. 2009. The role of the stratosphere in the European climate response to El Niño. *Nature Geoscience* **2**(1): 32–36.

Kinnersley J, Tung K. 1999. Mechanisms for the extratropical QBO in circulation and ozone. *J. Atmos. Sci.* **56**(12): 1942–1962.

Kodera K, Chiba M, Koide H, Kitoh A, Nikaidou Y. 1996. Interannual variability of the winter stratosphere and troposphere in the Northern Hemisphere. *J. Meteor. Soc. Japan* **74**(3): 365–382.

Kolstad E, Breiteig T, Scaife A. 2010. The association between stratospheric weak polar vortex events and cold air outbreaks in the Northern Hemisphere. *Q. J. R. Meteorol. Soc.* **136**(649): 886–893.

Labitzke K. 1982. On the interannual variability of the middle stratosphere during the northern winters. *J. Meteor. Soc. Japan* **60**: 124–139.

Labitzke K. 1987. Sunspots, the QBO, and the stratospheric temperature in the north polar region. *Geophys. Res. Lett.* **14**(5): 535–537.

Labitzke K. 2005. On the solar cycle-QBO relationship: a summary. *Journal of Atmospheric and Solar-Terrestrial Physics* **67**(1-2): 45–54.

Labitzke K, Van Loon H. 1989. The Southern Oscillation. Part IX: The influence of volcanic eruptions on the Southern Oscillation in the stratosphere. *J. Climate* **2**: 1223–1229.

Lahoz W. 2000. Northern Hemisphere winter stratospheric variability in the Met. Office Unified Model. *Q. J. R. Meteorol. Soc.* **126**(568): 2605–2630.

Leloup J, Lengaigne M, Boulanger J. 2008. Twentieth century ENSO characteristics in the IPCC database. *Climate Dynamics* **30**(2): 277–291.

Li D, Shine K, Gray L. 1995. The role of ozone-induced diabatic heating anomalies in the quasi-biennial oscillation. *Q. J. R. Meteorol. Soc.* **121**(524): 937–943.

Limpasuvan V, Thompson D, Hartmann D. 2004. The life cycle of the Northern Hemisphere sudden stratospheric warmings. *J. Climate* **17**: 2584–2596.

Lindzen R, Holton J. 1968. A theory of the quasi-biennial oscillation. *J. Atmos. Sci.* **25**: 1095–1107.

Lu C, Liu Y, Liu C. 2011. Middle atmosphere response to ENSO events in Northern Hemisphere winter by the Whole Atmosphere Community Climate Model. *Atmosphere-Ocean* **49**(2): 95–111, doi:10.1080/07055900.2011.576451.

Lu H, Baldwin M, Gray L, Jarvis M. 2008. Decadal-scale changes in the effect of the QBO on the northern stratospheric polar vortex. *J. Geophys. Res.* **113**: D10114, doi:10.1029/2007JD009647.

Manzini E, Giorgetta M, Esch M, Kornblueh L, Roeckner E. 2006. The influence of sea surface temperatures on the northern winter stratosphere: Ensemble simulations with the MAECHAM5 model. *J. Climate* **19**(16): 3863–3881.

Marshall A, Scaife A. 2009. Impact of the QBO on surface winter climate. *J. Geophys. Res.* **114**: D18110, doi:10.1029/2009JD011737.

Martin G, Bellouin N, Collins W, Culverwell I, Halloran P, Hardiman S, Hinton T, Jones C, McDonald R, McLaren A, *et al.* 2011. The HadGEM2 family of Met Office Unified Model Climate configurations. *Geoscientific Model Development Discussions* **4**: 765–841.

Mathieu P, Sutton R, Dong B, Collins M. 2004. Predictability of winter climate over the North Atlantic European region during ENSO events. *J. Climate* **17**(10): 1953–1974.

Matthes K, Langematz U, Gray L, Kodera K, Labitzke K. 2004. Improved 11-year solar signal in the Freie Universität Berlin Climate Middle Atmosphere Model (FUB-CMAM). *J. Geophys. Res.* **109**: D06101, doi:10.1029/2003JD004012.

Matthewman N, Esler J, Charlton-Perez A, Polvani L. 2009. A new look at stratospheric sudden warmings. Part III: Polar vortex evolution and vertical structure. *J. Climate* **22**(6): 1566–1585.

Maycock A, Keeley S, Charlton-Perez A, Doblas-Reyes F. 2011. Stratospheric circulation in seasonal forecasting models: implications for seasonal prediction. *Climate Dynamics* **36**(1): 309–321.

McIntyre M. 1982. How well do we understand the dynamics of stratospheric warmings. *J. Meteor. Soc. Japan* **60**: 37–65.

Mitchell D, Charlton-Perez A, Gray L. 2011a. Characterising the variability and extremes of the stratospheric polar vortices using 2D moments. *J. Atmos. Sci.* **68**: 1194–1213, doi:10.1175/2010JAS3555.1.

Mitchell D, Gray L, Charlton-Perez A. 2011b. The structure and evolution of the stratospheric vortex in response to natural forcings. *J. Geophys. Res.* **116**: D15110, doi:10.1029/2011JD015788.

Mitchell DM. 2010. Extreme variability of the stratospheric polar vortex. PhD thesis, University of Reading.

Naito Y, Hirota I. 1997. Interannual variability of the northern winter stratospheric circulation related to the QBO and the solar cycle. *J. Meteor. Soc. Japan* **75**(4): 925–937.

Naoe H, Shibata K. 2010. Equatorial quasi-biennial oscillation influence on northern winter extratropical circulation. *J. Geophys. Res.* **115**: D19102, doi:10.1029/2009JD012952.

Niwano M, Takahashi M. 1998. The influence of the equatorial QBO on the Northern Hemisphere winter circulation of a GCM. *J. Meteor. Soc. Japan* **76**(3): 453–461.

Norton W. 2003. Sensitivity of Northern Hemisphere surface climate to simulation of the stratospheric polar vortex. *Geophys. Res. Lett.* **30**(12): 1627, doi:10.1029/2003GL016958.

Osprey S, Gray L, Hardiman S, Butchart N, Bushell A, Hinton T. 2010. The climatology of the middle atmosphere in a vertically extended version of the Met Office's climate model. Part II: Variability. *J. Atmos. Sci.* **67**(11): 3637–3651.

Osprey S, Gray L, Hardiman S, Butchart N, Hinton T. 2011. Stratospheric variability in CMIP5 historical simulations of the Met Office climate model: High-top versus low-top. *J. Climate* In preparation.

O'Sullivan D, Dunkerton T. 1994. Seasonal development of the extratropical QBO in a numerical model of the middle atmosphere. *J. Atmos. Sci.* **51**(24): 3706–3706.

O'Sullivan D, Salby M. 1990. Coupling of the quasi-biennial oscillation and the extratropical circulation in the stratosphere through planetary wave transport. *J. Atmos. Sci.* **47**(5): 650–673.

O'Sullivan D, Young R. 1992. Modeling the quasi-biennial oscillation's effect on the winter stratospheric circulation. *J. Atmos. Sci.* **49**(24): 2437–2448.

Pascoe C, Gray L, Crooks S, Juckes M, Baldwin M. 2005. The quasi-biennial oscillation: Analysis using ERA-40 data. *J. Geophys. Res.* **110**: D08105, doi:10.1029/2004JD004941.

Plumb R. 1977. The interaction of two internal waves with the mean flow: Implications for the theory of the quasi-biennial oscillation. *J. Atmos. Sci.* **34**: 1847–1858.

Plumb R. 1984. The quasi-biennial oscillation. In: *Dynamics of the Middle Atmosphere*, vol. 1. p. 217.

Plumb R, Bell R. 1982. A model of the quasi-biennial oscillation on an equatorial beta-plane. *Q. J. R. Meteorol. Soc.* **108**(456): 335–352.

Polvani L, Kushner P. 2002. Tropospheric response to stratospheric perturbations in a relatively simple general circulation model. *Geophys. Res. Lett.* **29**(7), doi:10.1029/2001GL014284.

Press W, Flannery B, Teukolsky S, Vetterling W. 1992. *Numerical Recipes in C*. Cambridge University Press, 2 edn.

Randel W, Wu F, Swinbank R, Nash J, O'Neill A. 1999. Global QBO circulation derived from UKMO stratospheric analyses. *J. Atmos. Sci.* **56**(4): 457–474.

Ren R, Cai M, Xiang C, Wu G. 2011. Observational evidence of the delayed response of stratospheric polar vortex variability to ENSO SST anomalies. *Climate Dynamics* doi:10.1007/s00382-011-1137-7.

Richter JH, Matthes K, Calvo N, Gray LJ. 2011. Influence of the quasi-biennial oscillation and El Nino Southern Oscillation on the frequency of sudden stratospheric warmings. *J. Geophys. Res.* doi:10.1029/2011JD015757. In press.

Rigby MHN. 2010. Northern hemisphere winter stratospheric flow regimes. PhD thesis, University of Oxford.

Ruzmaikin A, Feynman J, Jiang X, Yung Y. 2005. Extratropical signature of the quasi-biennial oscillation. *J. Geophys. Res.* **110**: D11111, doi:10.1029/2004JD005382.

Sassi F, Kinnison D, Boville B, Garcia R, Roble R. 2004. Effect of El Nino–Southern Oscillation on the dynamical, thermal, and chemical structure of the middle atmosphere. *J. Geophys. Res.* **109**(D17): D17108, doi:10.1029/2003JD004434.

Scaife A, Knight J. 2008. Ensemble simulations of the cold European winter of 2005-2006. *Q. J. R. Meteorol. Soc.* **134**(636): 1647–1659.

Scaife A, Knight J, Vallis G, Folland C. 2005. A stratospheric influence on the winter NAO and North Atlantic surface climate. *Geophys. Res. Lett.* **32**(18): L18715, doi:10.1029/2005GL023226.

Schimanke S, Körper T, Spangehl T, Cubasch U. 2010. Multi-decadal variability of sudden stratospheric warmings in an AOGCM. *Geophys. Res. Lett.* **38**: L01801, doi:10.1029/2010GL045756.

Shaw T, Shepherd T. 2008. Atmospheric science: Raising the roof. *Nature Geoscience* **1**(1): 12–13.

Shine K. 1987. The middle atmosphere in the absence of dynamical heat fluxes. *Q. J. R. Meteorol. Soc.* **113**: 603–633.

Smith KL, Fletcher CG, Kushner PJ. 2010. The role of linear interference in the annular mode response to extratropical surface forcing. *J. Climate* **23**(22): 6036–6050, doi:10.1175/2010JCLI3606.1.

Taguchi M, Hartmann DL. 2006. Increased occurrence of stratospheric sudden warmings during El Niño as simulated by WACCM. *J. Climate* **19**(3): 324–332.

Thompson D, Baldwin M, Wallace J. 2002. Stratospheric connections to Northern Hemisphere wintertime weather: Implications for prediction. *J. Climate* **15**: 1421–1428.

Thompson D, Baldwin M, Wallace J. 2010. Stratospheric connection to Northern Hemisphere wintertime weather: Implications for prediction. *J. Climate* **15**: 1421–1428, doi:10.1175/1520-0442(2002)015¡1421:SCTNHW¿2.0.CO;2.

Thompson D, Wallace J. 1998. The Arctic Oscillation signature in the wintertime geopotential height and temperature fields. *Geophys. Res. Lett.* **25**(9): 1297–1300.

Thompson D, Wallace J. 2000. Annular modes in the extratropical circulation. Part I: Month-to-month variability. *J. Climate* **13**(5): 1000–1016.

Uppala S, Kållberg P, Simmons A, Andrae U, Bechtold V, Fiorino M, Gibson J, Haseler J, Hernandez A, Kelly G, *et al.* 2005. The ERA-40 re-analysis. *Q. J. R. Meteorol. Soc.* **131**(612): 2961–3012.

van Loon H, Labitzke K. 1987. Southern Oscillation. Part V. The anomalies in the lower stratosphere of the northern hemisphere in winter and a comparison with quasi-biennial oscillation. *Mon. Weather Rev.; (United States)* **115**: 357–369.

van Loon H, Madden R. 1981. The Southern Oscillation. Part I: Global associations with pressure and temperature in northern winter. *Mon. Wea. Rev.* **109**: 1150–1162.

von Storch H, Zwiers FW. 1999. *Statistical analysis in climate research*. Cambridge University Press.

Wallace J, Chang F. 1982. Interannual variability of the wintertime polar vortex in the Northern Hemisphere middle stratosphere. *Meteorological Society of Japan, Journal* **60**: 149–155.

Wallace J, Panetta R, Estberg J. 1993. Representation of the equatorial stratospheric quasi-biennial oscillation in EOF phase space. *J. Atmos. Sci.* **50**: 1751–1762.

Waugh D. 1997. Elliptical diagnostics of stratospheric polar vortices. *Q. J. R. Meteorol. Soc.* **123**: 1725–1748.

Wei K, Chen W, Huang R. 2007. Association of tropical Pacific sea surface temperatures with the stratospheric Holton-Tan oscillation in the Northern Hemisphere winter. *Geophys. Res. Lett.* **34**: L16814, doi:10.1029/2007GL030478.

Yamashita Y, Akiyoshi H, Takahashi M. 2011. Dynamical response in the northern hemisphere midlatitude and high-latitude winter to the QBO simulated by CCSR/NIES CCM. *J. Geophys. Res.* **116**: D06118, doi:10.1029/2010JD015016.